Restoring isotropy in a three-dimensional lattice model: The Ising universality class

Martin Hasenbusch [*]

Institut für Theoretische Physik, Universität Heidelberg, Philosophenweg 19, 69120 Heidelberg, Germany

We study a generalized Blume-Capel model on the simple cubic lattice. In addition to the nearest-neighbor coupling there is a next-to-next-to-nearest-neighbor coupling. In order to quantify spatial anisotropy, we determine the correlation length in the high-temperature phase of the model for three different spatial directions. It turns out that the spatial anisotropy depends very little on the dilution or crystal-field parameter D of the model and is essentially determined by the ratio of the nearest-neighbor and the next-to-next-to-nearest-neighbor coupling. This ratio is tuned such that the leading contribution to the spatial anisotropy is eliminated. Next we perform a finite-size scaling (FSS) study to tune D such that also the leading correction to scaling is eliminated. Based on this FSS study, we determine the critical exponents $\nu = 0.629\,98(5)$ and $\eta = 0.036\,284(40)$, which are in nice agreement with the more accurate results obtained by using the conformal bootstrap method. Furthermore, we provide accurate results for fixed-point values of dimensionless quantities such as the Binder cumulant and for the critical couplings. These results provide the groundwork for broader studies of universal properties of the three-dimensional Ising universality class.

I. INTRODUCTION

Studying spin models in the neighborhood of the critical temperature numerically, the presence of corrections to scaling hampers the extraction of universal quantities. The straightforward approach to reduce the effect of corrections to scaling is to simulate larger and larger lattices. It is more economic to study a family of models, and tune one or more parameters of the family such that the amplitude of the leading correction vanishes. This idea dates back to [1,2], where it is implemented by using high-temperature series expansions. The idea had been picked up in finite-size scaling (FSS) [3] studies using Monte Carlo simulations in Refs. [4–6], where the universality class of the three-dimensional Ising model had been studied. The idea has been applied successfully to the XY [7–10], the Heisenberg [11–13], and the disordered Ising [14] universality classes in three dimensions, resulting in accurate estimates of critical exponents. Note that the related improvement program initiated by Symanzik [15] is an indispensable building block in today's lattice QCD simulations. An open question is whether this program can be extended successfully to subleading corrections. Here we do not answer this question in general but consider one particular case. We study a lattice model with a second-order phase transition in the universality class of the three-dimensional Ising model. We extend the idea of eliminating corrections to scaling to subleading corrections that are caused by spatial anisotropy.

In the last years, the conformal bootstrap (CB) method brought enormous progress in the study of critical phenomena in three dimensions. In contrast to previous methods, the starting point is not a Hamiltonian. Instead, conformal invariance

and qualitative features of the fixed point are the basis of the analysis. The program has provided highly accurate results for critical exponents and for operator product expansion coefficients. For a recent review see, for example, Ref. [16]. In particular, in the case of the three-dimensional Ising universality class, detailed information on correction exponents is provided. See Table 2 of Ref. [17].

In a finite-size scaling study, the spatial anisotropy of the system leads to corrections that vanish like $L^{-\omega_{NR}}$, where $\omega_{NR} = 2.0208(12)$ [18,19] and L is the linear size of the system. The scaling field method [20] predicts a subleading correction with the correction exponent $\omega' = 1.67(11) < \omega_{NR}$ for the three-dimensional Ising universality class. Based on this result, it seemed of little use in the numerical study to eliminate the spatial anisotropy by tuning the parameters of the reduced Hamiltonian. However, the CB method, consistent with the functional renormalization group (FRG) (see, for example, Ref. [21]) indicates that $\omega' = 1.67(11)$ is an artifact of the scaling field method. For a more detailed discussion, see Sec. III below.

Based on this observation it seems promising to study reduced Hamiltonians, where in addition to the leading correction to scaling, the spatial anisotropy is eliminated to leading order. To this end, we study the Blume-Capel model on the simple cubic lattice, where in addition to the nearest-neighbor coupling, there is a third-nearest-neighbor coupling. This model has two parameters that can be tuned to remove corrections to scaling: the ratio of the two coupling constants and the parameter D that controls the density of vacancies. The definition of the model is given below in Sec. II.

The leading correction to scaling is eliminated by using a finite-size scaling study similar to our previous work (see [13] and references therein). In order to quantify the spatial anisotropy, we study the correlation length in the

high-temperature phase in different spatial directions. Finite-size scaling is less practical since the rotational invariance is not only broken at the microscopic scale by the lattice, but also at large length scales by the torus geometry of the lattice with periodic boundary conditions. This can be seen in two-point correlation functions even at rather small distances (see, for example, [22]). Instead, we study the correlation length in the high-temperature phase, where the parameters of the reduced Hamiltonian are chosen such that $L \gg \xi$. This way, the correlation functions at scales $\sim \xi$ are very little affected by the global torus geometry. In the high-temperature phase of the Ising model and related models, the correlation length can be determined very accurately by using a variance-reduced estimator of the two-point correlation function that is associated with the cluster algorithm [23,24].

Based on the FSS analysis, we get very accurate estimates of the critical exponents ν and η that are fully consistent with the CB estimates. Furthermore, we get very accurate results for the inverse critical temperature, which is valuable input for future studies of the model discussed here. Reduced spatial anisotropy should be, for example, helpful in the study of interfaces in the low-temperature phase or the thermodynamic Casimir effect with nontrivial geometries. Here we mostly delve into specifics of critical phenomena. For general reviews on critical phenomena and the renormalization group (RG) theory see, for example, [25–28].

The outline of the paper is the following: In Sec. II we define the model. In Sec. III follows a more detailed discussion on corrections to scaling. In Sec. IV we determine the ratio of nearest- and next-to-next-to-nearest-neighbor couplings that restores isotropy to leading order. To this end we study the correlation length in different directions in the high-temperature phase of the model. In Sec. V, by using FSS, we determine the value D^* of the dilution parameter, where leading corrections to scaling are eliminated. Based on this FSS study we obtain accurate estimates of critical exponents. Finally, we summarize and conclude.

II. THE MODEL

We study a generalized Blume-Capel model on the simple cubic lattice, where in addition to the nearest-neighbor coupling, there is a nonvanishing third-nearest-neighbor coupling. This model has been discussed, for example, in Ref. [4]. See in particular Eq. (2) of Ref. [4]. For a vanishing external field, it is defined by the reduced Hamiltonian

$$H = -K_1 \sum_{\langle xy \rangle} s_x s_y - K_3 \sum_{[xy]} s_x s_y + D \sum_x s_x^2, \qquad (1)$$

where the spin s_x might assume the values $s_x \in \{-1, 0, 1\}$. $x = (x^{(0)}, x^{(1)}, x^{(2)})$ denotes a site on the simple cubic lattice, where $x^{(i)} \in \{0, 1, \ldots, L_i - 1\}$. Furthermore, $\langle xy \rangle$ denotes a pair of nearest-neighbor and $[xy]$ a pair of next-to-next-to-nearest-neighbor, or third-nearest neighbor on the lattice. In this study we consider $L_0 = L_1 = L_2 = L$ and periodic boundary conditions throughout. Here we refer to D as dilution parameter. In the literature, D is also denoted as crystal-field parameter. The partition function is given by $Z = \sum_{\{s\}} \exp(-H)$, where the sum runs over all spin configurations. In the following we denote the ratio of coupling

constants as

$$q_3 = K_3/K_1. \qquad (2)$$

For $q_3 = 0$, the model has been thoroughly studied in the literature. See [29] and references therein. In the limit $D \to -\infty$, the vacancies $s_x = 0$ are completely suppressed, and the Ising model is recovered. For $D < D_{\mathrm{tri}}$, the model undergoes a second-order phase transition in the universality class of the three-dimensional Ising model. For $D > D_{\mathrm{tri}}$, there is a first-order phase transition. Along the line of second-order transitions, the amplitude of leading corrections depends on the parameter D. It has been demonstrated numerically that there is a value D^* of the parameter, where leading corrections to scaling vanish. In Ref. [29] we find $D^* = 0.656(20)$, which is clearly smaller than $D_{\mathrm{tri}} = 2.0313(4)$ [30]. For a more detailed discussion see Ref. [29].

For the model, Eq. (1), for $q_3 \geqslant 0$, we expect that there is a critical plane given by $K_{1,c}(D, q_3)$ that is bounded by a line of tricritical transitions $D_{\mathrm{tri}}(q_3)$. On the critical plane, there should be a line $D^*(q_3)$, where leading corrections to scaling vanish. There should be also a line, where the isotropy is restored to leading order. It is best represented by $q_3^{\mathrm{iso}}(D)$ since we expect that $q_3^{\mathrm{iso}}(D)$ depends only little on D, which is confirmed by our numerical results discussed below. These two lines might have a crossing, where both corrections to scaling vanish.

In Ref. [4] as well as in the more recent papers [31,32], the Ising model, corresponding to $D \to -\infty$, with nearest- and next-to-next-to-nearest-neighbor couplings had been studied. It turns out that the amplitude of leading corrections to scaling depends on the ratio q_3. In particular, there is a value q_3^*, where leading corrections to scaling vanish. The authors of Refs. [4,31,32] performed a finite-size scaling analysis based on the quantity $Q = \langle m^2 \rangle^2 / \langle m^4 \rangle$, where m is the magnetization. Note that Q is the inverse of the Binder cumulant defined here, Eq. (20), for $j = 2$. In Table III of Ref. [32] the estimates $b_1 = 0.097(2), 0.051(2), 0.0118(20), -0.0180(20)$, and $-0.0480(20)$ for $q_3 = 0, 0.1, 0.2, 0.3$, and 0.4, respectively, are given, where b_1 denotes the amplitude of the leading correction. Interpolating linearly, we arrive at $q_3^* = 0.24(1)$.

Assuming that $D^*(q_3)$ is monotonically decreasing with increasing q_3, the crossing of $q_3^{\mathrm{iso}}(D)$ and $D^*(q_3)$ exists if $q_3^{\mathrm{iso}}(-\infty) \leqslant q_3^*$. Hence, as a first step of our numerical study, we determine $q_3^{\mathrm{iso}}(-\infty)$.

In the following we approach the critical line keeping q_3 constant. Therefore, we use the parametrization

$$\begin{aligned} K_1 &= K, \\ K_3 &= q_3 K. \end{aligned} \qquad (3)$$

III. CORRECTIONS TO SCALING

Field-theoretic methods and high-temperature series expansions and Monte Carlo simulations of lattice models give consistently for the leading correction to scaling exponent $\omega \approx 0.8$ for the three-dimensional Ising universality class. For a summary of results see, for example, Table 19 of [25]. The most accurate result $\omega = 0.829\,68(23)$, is obtained by using the CB method [17]. Note that in Table 2 of Ref. [17]

dimensions Δ of operators are given. In the case of the leading correction, $\omega = \Delta_{\epsilon'} - 3$ holds.

Before the advent of the CB method, information on subleading corrections had been scarce. The ϵ expansion and perturbation theory in three dimensions fixed do not provide information on subleading corrections. In principle, Monte Carlo renormalization group (MCRG) methods (see, for example, Refs. [33–37]) are capable of producing such results. However, these are not given in the literature. Note that in these studies the error of the correction exponent ω is considerably larger than that of the critical exponents. Obtaining the result for subleading corrections should be even harder.

In previous work (for example, Ref. [29]), we assumed that the results obtained in Ref. [20] by using the scaling field method on subleading corrections to scaling are correct. It predicts a subleading correction with $\omega' = 1.67(11)$. This result is in contradiction with results obtained by using functional renormalization group methods. Depending on the approximation scheme that is used, results $2.838 \leqslant \omega' \leqslant 3.6845$ are, for example, obtained in Ref. [21]. Recent work [17], using the conformal bootstrap method gives $\omega' = \Delta_{\epsilon''} - 3 = 3.8956(43)$. It seems that $\omega' = 1.67(11)$ is an artifact of the scaling field method.

There is a correction due to the fact that the simple cubic lattice breaks the spatial isotropy. This phenomenon can already be observed in the context of partial differential equations. See, for example, Ref. [38], where the Laplacian on a square and a simple cubic lattice is discussed. These results directly apply to free field theory on the lattice. Hence, for free field theory on the simple cubic lattice we get $\omega_{NR,\mathrm{free}} = 2$ and $q_{3,\mathrm{free}}^{\mathrm{iso}} = \frac{1}{8}$.

In the case of the three-dimensional Ising universality class one gets $\omega_{NR} = 2.0208(12)$ (see Table 1 of [18]) or by using the CB method $\omega_{NR} = \Delta_{C_{\mu\nu\rho\sigma}} - 3 = 2.022\,665(28)$, given in Table 2 of Ref. [17]. Note that the value of the correction exponent differs only by little from the free field value. Also, the value of q_3^{iso} that we find below differs only by little from the free field value. This fact is a bit surprising since q_3^{iso} should depend on the details of the model.

Our numerical analysis relies on the fact that amplitudes of corrections to scaling are smooth functions of the parameters of the reduced Hamiltonian, as it is predicted by RG theory. Furthermore, following RG theory, ratios of correction amplitudes in different quantities, for the same type of correction, are universal. (For a discussion see, for example, Sec. 1.5 of Ref. [25].) This fact in particular implies that corrections in different quantities vanish at the same values, in our case $(q_3^{\mathrm{iso}}, D^*)$, of parameters of the reduced Hamiltonian.

IV. RESTORING ISOTROPY

Our numerical study consists of two essentially separate parts. Following the hypothesis that $q_3^{\mathrm{iso}}(D)$ depends only little on D, we first determine q_3^{iso} for the Ising limit $D \to -\infty$. Then we perform a preliminary finite-size scaling study to get an estimate of $D^*(q_3^{\mathrm{iso}}(-\infty))$. For this estimate we determine again q_3^{iso}. Since this estimate indeed differs very little from $q_3^{\mathrm{iso}}(-\infty)$, we regard it as our final estimate. In the second part of our study we perform an extensive FSS study to determine $D^*(q_3^{\mathrm{iso}})$ accurately.

The simulations in the high-temperature phase of the Ising model were performed by using the single-cluster algorithm [24]. In the case of the Blume-Capel model with finite D, local updates that allow the transition from $s_x = 0$ to ± 1 and vice versa were used in addition. For a more detailed discussion of such a hybrid update scheme see, for example, Sec. 5 of Ref. [39].

A. Correlation length in the high-temperature phase

In order to quantify spatial anisotropy, we determine the correlation length in three different directions of the lattice. Below we discuss how the correlation length is determined. We start with the definition of the basic quantities. We define slice averages

$$S(x_0) = \sum_{x_1,x_2} s_x, \tag{4}$$

where the slice is perpendicular to the $(1,0,0)$ axis. In addition, we consider slices perpendicular to the $(1,1,0)$ and the $(1,1,1)$ axes. The corresponding slice averages are given by

$$\tilde{S}_{x_0} = \sum_{x_1,x_2} s_{x_0-x_1,x_1,x_2} \tag{5}$$

and

$$\bar{S}_{x_0} = \sum_{x_1,x_2} s_{x_0-x_1-x_2,x_1,x_2}. \tag{6}$$

Note that the arithmetics of the coordinates is understood modulo the linear lattice size L. The distance between adjacent slices is $d_s = 1, 2^{-1/2}$, and $3^{-1/2}$ for slices perpendicular to the $(1,0,0)$, $(1,1,0)$, and the $(1,1,1)$ axis, respectively. The slice correlation function is defined as

$$G(t) = \langle S(x_0)S(x_0 + t) \rangle. \tag{7}$$

Also here $x_0 + t$ is understood modulo the linear lattice size L. The correlation functions $\tilde{G}(t)$ and $\bar{G}(t)$ are defined analogously.

In our simulations, in order to reduce the statistical error, we average over all x_0 and all directions equivalent to those given by the $(1,0,0)$, $(1,1,0)$, and the $(1,1,1)$ axis, respectively. The correlation function is determined by using the variance-reduced estimator associated with the cluster algorithm [23,24].

We define the effective correlation length

$$\xi_{\mathrm{eff}}(t) = \frac{d_s}{\ln[G(t)/G(t+1)]}, \tag{8}$$

where $L \gg t$ is assumed and d_s is the distance between adjacent slices. To relax $L \gg t$ to some extent, we take the periodicity of the lattice into account. To this end we solve numerically

$$G(t) = c\left[\exp\left(-\frac{d_s t}{\xi_{\mathrm{eff}}(t)}\right) + \exp\left(-\frac{d_s(L-t)}{\xi_{\mathrm{eff}}(t)}\right)\right], \tag{9}$$

$$G(t+1) = c\left[\exp\left(-\frac{d_s(t+1)}{\xi_{\mathrm{eff}}(t)}\right) + \exp\left(-\frac{d_s(L-t-1)}{\xi_{\mathrm{eff}}(t)}\right)\right] \tag{10}$$

TABLE I. Results for the correlation length of the Ising model with $q_3 = 0$. In the first column we give the coupling K, in the second column we give the linear lattice size L, and in the third column the correlation length ξ parallel to the (1,0,0) axis. Then, follow the ratios r_2 and r_3 defined in Eq. (11).

K	L	$\xi_{(1,0,0)}$	r_2	r_3
0.2	40	2.04147(4)	1.004922(7)	1.006606(8)
0.20944	60	2.99993(4)	1.002281(4)	1.003056(5)
0.21376	80	3.99868(4)	1.001281(3)	1.001715(3)
0.2161	100	5.02713(13)	1.000802(8)	1.001083(10)
0.21743	120	6.00095(9)	1.000562(4)	1.000757(5)
0.21896	160	8.01343(17)	1.000321(6)	1.000426(7)

TABLE II. We give results for the correlation length of the Blume-Capel model at $q_3 = 0$ and $D = 0.655$. In the first column we give the coupling K, in the second column we give the linear lattice size L, and in the third column the correlation length $\xi_{(1,0,0)}$ parallel to the (1,0,0) axis. Then, follow the ratios r_2 and r_3 defined in Eq. (11).

K	L	$\xi_{(1,0,0)}$	r_2	r_3
0.3568	40	1.99990(5)	1.005124(8)	1.006871(9)
0.3713	60	3.00874(5)	1.002269(4)	1.003026(5)
0.37721	80	4.00087(6)	1.001282(4)	1.001709(4)
0.3804	100	5.03495(8)	1.000804(3)	1.001072(4)
0.38217	120	6.00109(10)	1.000569(3)	1.000754(4)
0.38337	140	7.00206(10)	1.000418(3)	1.000555(4)
0.3842	160	8.00502(10)	1.000317(3)	1.000424(3)
0.3848	180	9.00819(13)	1.000251(3)	1.000336(3)

with respect to $\xi_{\mathrm{eff}}(t)$. For the Ising universality class in three dimensions, in the high-temperature phase, $\xi_{\mathrm{eff}}(t)$ converges quickly as $t \to \infty$. See Ref. [39] and references therein.

In a set of preliminary simulations, we determined the lattice size L and distance t that is needed to keep deviations from the desired limit $L \to \infty$ followed by $t \to \infty$ at a size smaller than the statistical error. We conclude that $d_s t \simeq 2\xi$ and $L \simeq 20\xi$ is sufficient. In the following we take $\xi_{\mathrm{eff}}(t)$ at $d_s t \simeq 2\xi$ as estimate of the correlation length ξ. The direction is indicated by a subscript.

In order to quantify the spatial anisotropy, we study the ratios

$$r_2 = \frac{\xi_{(1,0,0)}}{\xi_{(1,1,0)}}, \quad r_3 = \frac{\xi_{(1,0,0)}}{\xi_{(1,1,1)}} \tag{11}$$

in the neighborhood of the critical point.

B. Numerical results for the Ising model and the Blume-Capel model with nearest-neighbor coupling only

First we simulated the standard Ising model in the high-temperature phase. The behavior of the correlation length is given by

$$\xi = a(K_c - K)^{-\nu}[1 + c(K_c - K)^{\theta} + d(K_c - K) + \cdots], \tag{12}$$

where K_c, a, c, and d are nonuniversal constants. The critical exponent of the correlation length is $\nu = 1/y_t$, where y_t is the thermal renormalization group exponent. The correction exponent is $\theta = \nu\omega$. For numerical results of the second moment correlation length in the high-temperature phase of the Ising model with $q_3 = 0$ see, for example, Appendix of Ref. [40]. In Ref. [41] the accurate estimate $K_c = 0.221\,654\,626(5)$ is given.

In this study, we focus on $\xi < 10$. Our numerical results for the correlation length of the Ising model, $q_3 = 0$, are summarized in Table I. Note that in the case of the ratios r_2 and r_3, the statistical correlation between the correlation lengths in the different directions are properly taken into account by performing a jackknife analysis.

We fitted the data with the *Ansatz*

$$r_i - 1 = a\xi^{-x}, \tag{13}$$

where a and the exponent x are free parameters. We refer to $\xi_{(1,0,0)}$ as ξ to keep the notation simple. The statistical error of ξ is ignored for simplicity. Fitting all data for r_3 we get $x = 2.006(3)$ and $\chi^2/\mathrm{DOF} = 0.26$, where DOF is degrees of freedom. Adding a correction term $\propto L^{-2}$ we get $x = 2.016(12)$ and $\chi^2/\mathrm{DOF} = 0.10$ instead. We conclude that the exponent x is consistent with the results for ω_{NR} of Refs. [17,18]. However, our accuracy is by far lower than that of Ref. [17].

Next we have simulated the Blume-Capel model on the simple cubic lattice with $q_3 = 0$ at $D = 0.655$ at eight values of K that correspond to $\xi \approx 2, 3, 4, 5, 6, 7, 8,$ and 9. Our numerical results are given in Table II.

Fitting all data for r_3 with $\xi \geqslant 3$ by using the *Ansatz* (13) we get $x = 2.010(4)$ and $\chi^2/\mathrm{DOF} = 0.32$. Fitting all data with an *Ansatz* containing a correction term $\propto L^{-2}$ we get $x = 2.010(7)$ and $\chi^2/\mathrm{DOF} = 0.32$. Fixing $x = 2.022\,665$ in the *Ansatz* (13), we get very similar results for the amplitude a for both the Ising and the improved Blume-Capel models. We conclude that the spatial anisotropy depends little on the amplitude of leading corrections to scaling, as we conjectured in the beginning. This fact is illustrated in Fig. 1 were we plot $(r_2 - 1)\xi^{\omega_{NR}}$ and $(r_3 - 1)\xi^{\omega_{NR}}$ versus the correlation length ξ. The data for the two models fall essentially on top of each other.

C. Determination of q_3^{iso}

Next we determine q_3^{iso} for the Ising model, corresponding to $D \to -\infty$. Preliminary simulations give $q_3^{\mathrm{iso}} \approx \frac{2}{15}$. In order to get an accurate estimate of q_3^{iso}, we performed a number of simulations at $q_3 = \frac{1}{7}, \frac{2}{15},$ and $\frac{1}{8}$ for a correlation length up to $\xi \approx 6$. Our results are summarized in Table III.

Furthermore, we estimate D^* for $q_3 = \frac{2}{15}$. To this end, we performed a FSS study focusing on U_4 at $Z_a/Z_p = 0.5425$. For the definition of the Binder cumulant U_4 and the ratio of partition functions Z_a/Z_p see Sec. V below. Here we simulated lattices up to the linear size $L = 32$. We used $U^*_{4,Z_a/Z_p=0.5425} \approx 1.603\,57$ obtained in Sec. VI of Ref. [29] as input. We find $D^* \approx -0.43$. Based on this preliminary result, we performed simulations at $D = -0.43$ for $q_3 = \frac{2}{15}$ and $\frac{1}{8}$ in the high-temperature phase. The value of K is tuned such that the correlation length assumes the values $\xi \approx 2, 3, 4, 5, 6, 7,$ and 8. Our results are summarized in Table IV.
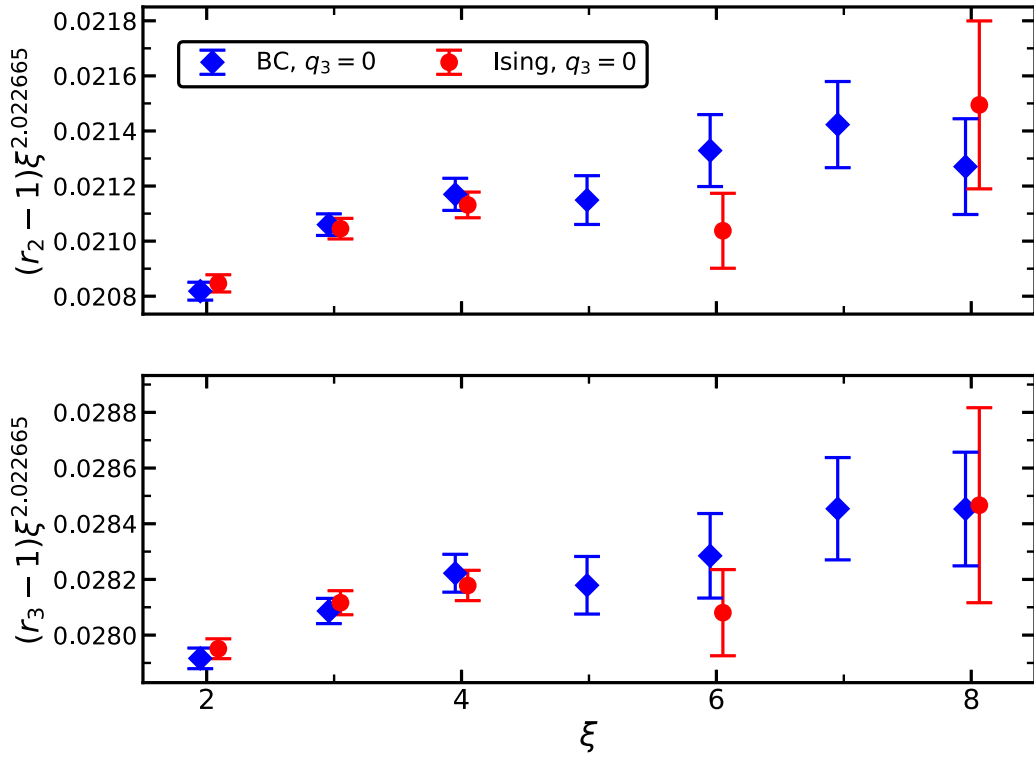
FIG. 1. We plot $(r_2 - 1)\xi^{\omega_{NR}}$ (upper part) and $(r_3 - 1)\xi^{\omega_{NR}}$ (lower part) for the Ising model and the Blume-Capel model at $D = 0.655$, both at $q_3 = 0$, versus the correlation length ξ. Note that the values on the x axis are slightly shifted to reduce the overlap of the Ising and the Blume-Capel data points. The two parts of the figure share the legend and the labeling of the x axis. Note the different scales on the y axis.

In Fig. 2 we plot $(r_2 - 1)\xi^{\omega_{NR}}$ and $(r_3 - 1)\xi^{\omega_{NR}}$ versus the correlation length ξ. With increasing ξ the values of $(r_2 - 1)\xi^{\omega_{NR}}$ and $(r_3 - 1)\xi^{\omega_{NR}}$ seem to approach a constant for both models and both values of q_3 we simulated at. It seems obvious that $\frac{1}{8} < q_3^{\text{iso}} < \frac{2}{15}$ for both models. The values of $(r_2 - 1)\xi^{\omega_{NR}}$ and $(r_3 - 1)\xi^{\omega_{NR}}$ are slightly larger for the Ising model, suggesting that q_3^{iso} is slightly larger for the Ising model than for the Blume-Capel model at $D = -0.43$.

In order to obtain a numerical estimate of q_3^{iso} for the Blume-Capel model at $D = -0.43$ we performed fits with the

Ansätze

$$r_3 - 1 = a\xi^{-\omega_{NR}} \tag{14}$$

and

$$r_3 - 1 = a\xi^{-\omega_{NR}} + b\xi^{-\omega'_{NR}}, \tag{15}$$

where we have fixed $\omega_{NR} = 2.022\,665$. In the case of the correction term we took either $\omega'_{NR} = 6.420\,65 - 3 = 3.420\,65$ (see Table 2 of Ref. [17]) or the *ad hoc* choice $\omega'_{NR} = 4$. For example, with the *Ansatz* (15) and $\omega'_{NR} = 3.420\,65$, taking $\xi \gtrsim 3$ we get $a = -0.000\,62(7)$ and $0.000\,73(7)$ for $q_3 = \frac{2}{15}$

TABLE III. We give results for the correlation length $\xi_{(1,0,0)}$ and the ratios r_2 and r_3 of the Ising model with $q_3 = \frac{1}{7}$, $\frac{2}{15}$, and $\frac{1}{8}$. L is the linear lattice size and K the coupling constant.

q_3	K	L	$\xi_{(1,0,0)}$	$r_2 - 1$	$r_3 - 1$
1/7	0.1556	40	2.02430(7)	−0.000410(12)	−0.000695(14)
1/7	0.16938	100	5.02654(24)	−0.000043(14)	−0.000055(16)
2/15	0.158	40	2.03501(3)	−0.000189(6)	−0.000372(7)
2/15	0.1663	60	3.02940(4)	−0.000056(5)	−0.000074(5)
2/15	0.16981	80	3.99996(6)	−0.000025(4)	−0.000028(5)
2/15	0.17175	100	5.00911(7)	−0.000008(4)	−0.000009(5)
2/15	0.172889	120	5.99953(9)	−0.000009(4)	−0.000004(5)
1/8	0.16	40	2.03256(3)	0.000041(6)	−0.000050(7)
1/8	0.1686	60	3.06724(4)	0.000043(5)	0.000058(5)
1/8	0.171951	80	3.99987(7)	0.000025(5)	0.000038(6)
1/8	0.1739	100	5.00231(10)	0.000033(6)	0.000047(7)
1/8	0.17506	120	5.99911(11)	0.000009(5)	0.000020(6)

TABLE IV. We give results for the correlation length $\xi_{(1,0,0)}$ and the ratios r_2 and r_3 of the Blume-Capel model at $D = -0.43$ with $q_3 = \frac{2}{15}$ and $\frac{1}{8}$. L is the linear lattice size and K the coupling.

q_3	K	L	$\xi_{(1,0,0)}$	$r_2 - 1$	$r_3 - 1$
2/15	0.2037	40	1.98782(3)	−0.000222(7)	−0.000431(7)
2/15	0.2144	60	3.00063(3)	−0.0000699(27)	−0.0001043(31)
2/15	0.2188	80	4.00152(3)	−0.0000344(19)	−0.0000494(22)
2/15	0.2211	100	5.00263(4)	−0.0000208(19)	−0.0000288(22)
2/15	0.22247	120	6.00387(5)	−0.0000140(19)	−0.0000227(22)
2/15	0.223356	140	6.99959(5)	−0.0000116(18)	−0.0000166(22)
2/15	0.223971	160	7.99879(6)	−0.0000067(18)	−0.0000081(21)
1/8	0.2065	40	2.00215(3)	0.0000136(52)	−0.0001107(60)
1/8	0.217	60	2.99516(3)	0.0000307(34)	0.0000290(39)
1/8	0.22147	80	4.00089(4)	0.0000275(28)	0.0000290(33)
1/8	0.2238	100	5.00716(4)	0.0000168(18)	0.0000215(22)
1/8	0.22517	120	5.99963(5)	0.0000116(19)	0.0000120(22)
1/8	0.226065	140	6.99452(5)	0.0000090(19)	0.0000120(22)
1/8	0.226687	160	7.99376(6)	0.0000070(19)	0.0000078(22)

and $\frac{1}{8}$, respectively. Note that q_3^{iso} is defined as the zero of a. Linearly interpolating we get $q_3^{\text{iso}} = 0.1295(3)$. Based on the fits that we performed by using the *Ansätze* (14) and (15) we quote

$$q_3^{\text{iso}} = 0.129(1) \tag{16}$$

as final result for the Blume-Capel model at $D = -0.43$. It is chosen such that the estimates, including their respective error bars, obtained by performing these fits are covered. We did not

repeat this analysis for r_2. However, just comparing the upper and lower parts of Fig. 2 by eye, it is clear that the outcome of such an analysis will be very similar.

Below we perform a thorough FSS study, resulting in $D^* = -0.380(5)$ for $q_3 = 0.129$. Since the difference of q_3^{iso} for the Blume-Capel model at $D = -0.43$ and the Ising model is small, we regard the result (16) as valid for the revised estimate of D^* and abstain from simulating again in the high-temperature phase of the Blume-Capel model at $D^* = -0.38$.
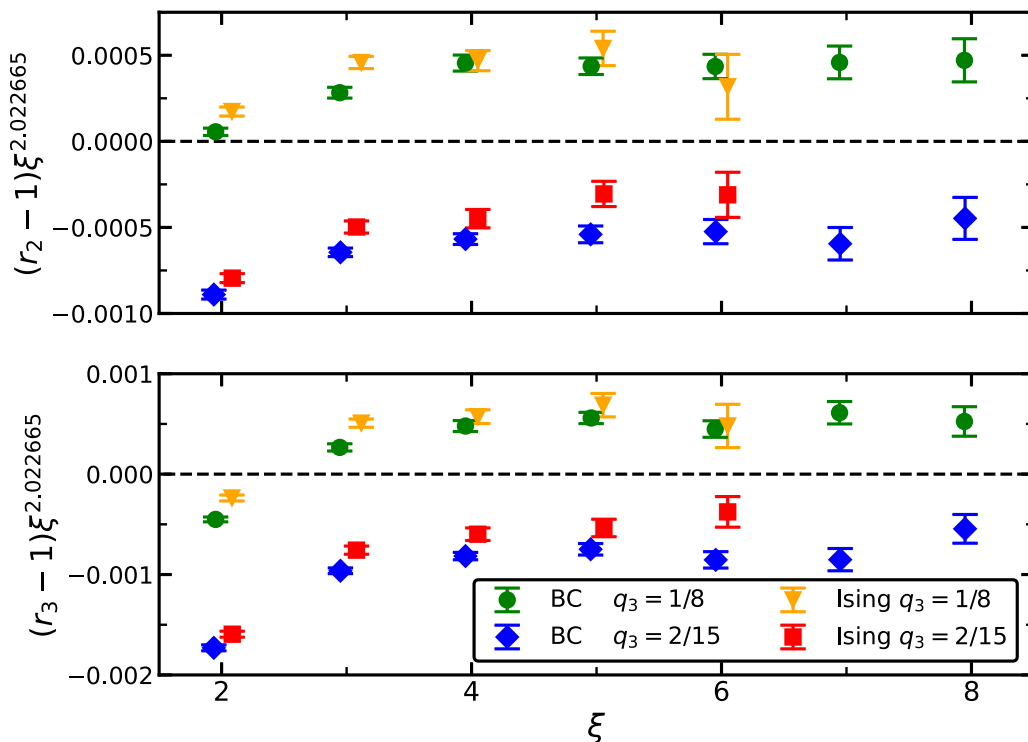

FIG. 2. We plot $(r_2 - 1)\,\xi^{2.022\,665}$ (upper part) and $(r_3 - 1)\,\xi^{2.022\,665}$ (lower part) versus the correlation length ξ for the Ising model and the Blume-Capel model at $D = -0.43$ at $q_3 = \frac{2}{15}$ and $\frac{1}{8}$. Note that the values on the x axis are slightly shifted to reduce the overlap of the Ising and the Blume-Capel model data points. The two parts of the figure share the legend and the labeling of the x axis. Note the different scales on the y axis.

From Fig. 1 we read off that $(r_3 - 1)\xi^{\omega_{NR}} \approx 0.029$ for the Ising model and the Blume-Capel model at $D = 0.655$ both at $q_3 = 0$ in the limit $\xi \to \infty$. Taking the results of the fits discussed above for the amplitude of $r_3 - 1$ at $q_3 = \frac{1}{8}$ and $\frac{2}{15}$ we get $d[(r_3 - 1)\xi^{\omega_{NR}}]/dq_3 \approx 0.0013/(\frac{1}{8} - \frac{2}{15}) = -0.156$ at $q_3 = q_3^{\mathrm{iso}}$. Hence, the error given in Eq. (16) means that for $q_3 = 0.129$, the leading violation of spatial isotropy is suppressed at least by a factor of about $0.029/(|-0.156| \times 0.001) \approx 180$ compared with $q_3 = 0$.

To get an idea of the statistics of our simulations let us briefly discuss the runs for $L = 160$, $q_3 = \frac{2}{15}$, and $D = -0.43$. In total we performed about 3.6×10^7 update cycles. Each cycle consists of one sweep with the local update algorithm followed by 12 000 single-cluster updates. The number of single-cluster updates is chosen such that this number times the average size of a cluster roughly equals half of the volume L^3 of the lattice. For parallelization, we performed 400 separate runs. For each run, we performed 10 000 update cycles for equilibration. In total these runs took about 6 months of CPU time on a single core of an AMD EPYC^{TM} 7351P CPU. In the simulations discussed in this section, we used the SIMD-oriented Fast Mersenne Twister (SFMT) algorithm [42] as random number generator.

Throughout this work, least-square fits were performed by using the function `curve_fit()` contained in the SCIPY library [43]. Plots were generated by using the MATPLOTLIB library [44].

V. FINITE-SIZE SCALING STUDY

In the second part of our numerical study we accurately determine D^* for $q_3 = 0.129$. The outline of the study follows closely our recent studies [10,13]. Therefore, we abstain from a detailed discussion of the theoretical background. Below we define the quantities that we measure during the simulation. It follows a brief discussion of the simulations that we performed. First, we analyze the dimensionless quantities to locate D^* and get accurate estimates of K_c for several values of D close to D^*. Next, we obtain accurate estimates of the critical exponents η and ν by analyzing the behavior of the magnetic susceptibility and the slopes of dimensionless quantities.

A. Quantities studied in finite-size scaling

The magnetic susceptibility χ for a vanishing magnetization and the second moment correlation length ξ_{2nd} are defined as

$$\chi = \frac{1}{V}\left\langle\left(\sum_x s_x\right)^2\right\rangle \tag{17}$$

and

$$\xi_{2nd} = \sqrt{\frac{\chi/F - 1}{4\sin^2 \pi/L}}, \tag{18}$$

where

$$F = \frac{1}{V}\left\langle\left|\sum_x \exp\left(i\frac{2\pi x_1}{L}\right)s_x\right|^2\right\rangle \tag{19}$$

is the Fourier transform of the correlation function at the lowest nonzero momentum. The Binder cumulant U_4 and its generalizations U_{2j} are defined as

$$U_{2j} = \frac{\langle(m^2)^j\rangle}{\langle m^2\rangle^j}, \tag{20}$$

where $m = \frac{1}{V}\sum_x s_x$ is the magnetization of the system. Furthermore, we study the ratio of partition functions Z_a/Z_p, where a denotes a system with antiperiodic boundary conditions in one of the directions and periodic ones in the remaining two directions, while p denotes a system with periodic boundary conditions in all directions. This quantity is computed by using the cluster algorithm. For a discussion see Appendix A 2 of Ref. [8].

The second moment correlation length ξ_{2nd}, the Binder cumulant U_4, its generalizations, and the ratio of partition functions Z_a/Z_p are dimensionless quantities or phenomenological couplings. In the following we denote these quantities by R_i. We obtain the critical exponent ν from the behavior of the slope of dimensionless quantities

$$S_{R_i} = \frac{\partial S_{R_i}}{\partial K}. \tag{21}$$

In the analysis discussed below, we need the quantities as a function of K in some neighborhood of the value $K_{\mathrm{sim}} \approx K_c$ of K that is used in the simulation. To this end, we compute the Taylor coefficients of the observables around K_{sim} up to third order.

For a discussion of corrections that are caused by the observable itself see, for example, Sec. 4 of Ref. [45]. The authors discuss the two-dimensional Ising model on the square lattice with periodic boundary conditions. The arguments brought forward should also apply to the present case. In particular, it is noted that one has to take into account the analytic background of the magnetic susceptibility. This leads to a correction in U_{2j} and ξ_{2nd}/L proportional to $L^{-(2-\eta)}$. In the case of ξ_{2nd}/L, there are in addition corrections that are proportional to L^{-2}. The ratio of partition functions has only corrections that decay exponentially in the linear lattice size.

B. Simulations

The simulations are performed by using a hybrid of local updates, single-cluster updates [24], and the wall-cluster update [6]. For each measurement, we performed one sweep with the local update, $L/4$ single-cluster updates, and one wall-cluster update. For a more detailed discussion of similar hybrid update schemes see, for example, Refs. [10,13]. We simulated the model for $q_3 = 0.129$ at $D = -0.3$, -0.35, -0.38, -0.4, -0.42, and -0.46. We simulated at good approximations of $K_c(D, q_3)$. These estimates were successively improved, while increasing the linear lattice size that is simulated.

For all values of D that we consider, we simulated the linear lattice sizes $L = 6, 7, 8, ..., 15, 16, 18, 20, ..., 32, 36, 40, 48, 56, ..., 72$. For $D = -0.3$, we simulated $L = 120$ in addition. For $D = -0.35, -0.4$, and -0.42 we simulated $L = 80, 100$, and 120 in addition. In the case of $D = -0.38$, we simulated $L = 80, 100, 120$, and 200 in addition.

In total we have spent the equivalent of about 90 years of CPU time on a single core of an AMD EPYC^{TM} 7351P CPU. To give the reader an idea of the statistics of our simulations: In the case of $D = -0.38$ we performed about 6.7×10^9 measurements for $L = 20$. This number decreases to 1.5×10^8 measurements for $L = 200$. As random number generator, we used either the SIMD-oriented fast Mersenne twister (SFMT) algorithm [42] or a modified KISS generator. A few simulations for $D = -0.38$ have been performed by using Lüscher's ranlux generator [46] for comparison. For more details, see Appendix A. Analyzing data and in particular estimating errors of the final results for critical exponents and other quantities of interest, we follow a cautious approach that we adopted over the years. It is spelled out, for example, in Sec. V of Ref. [10]. Essentially, we perform a number of different fits that we consider as reasonable. Then the final result and its error bar are chosen such that the results of these fits, including their respective error bars are covered. This obviously leads in general to a larger error bar compared with selecting one preferred fit and taking its result and error bar as the final one.

C. Dimensionless quantities

In a first step we performed a joint fit of the dimensionless quantities Z_a/Z_p, ξ_{2nd}/L, U_4, and U_6 for all values of D considered. As *Ansatz* we use

$$R_i(K_c, L) = R_i^* + b_i(D)L^{-\omega} + c_i(D)L^{-\epsilon_1} + d_i(D)L^{-\epsilon_2}. \quad (22)$$

We have omitted corrections $cb_i^2(D)L^{-2\omega}$ and higher powers since $b_i(D)$ is assumed to be small for the values of D that we consider.

In the case of ξ_{2nd}/L, U_4, and U_6 we expect that there are corrections due to the analytic background of the magnetic susceptibility. Hence, $\epsilon_1 = 2 - \eta$. In the case of ξ_{2nd}/L there is in addition $\epsilon_2 = 2$, as discussed in Sec. V A. We assume that corrections due to the violation of the rotational invariance can be ignored here. As a check, in the case of Z_a/Z_p, we assume one subleading correction with $\epsilon_1 = 2.022\,665$.

The renormalization group predicts that the ratio $b_i(D)/b_j(D)$ does not depend on D. In our fits, we used different parametrizations of $b_i(D)$. For example, the linear approximation

$$b_i(D) = a_i(D - D^*), \quad (23)$$

where a_i and D^* are free parameters. As check we added a quadratic term

$$b_i(D) = a_i[(D - D^*) + c(D - D^*)^2]. \quad (24)$$

The coefficients of subleading corrections are assumed either to be constant or linearly dependent on D. In a preliminary stage of the analysis we performed a number of fits using different *Ansätze* of the type discussed above, including different subsets of values of D. Note that by varying the range of D, we probe the validity of approximations such as Eqs. (23) and (24). Motivating our final results, we focus on three different *Ansätze* that we specify below. Note that these three fits essentially cover the range of results that we considered as reasonable in the preliminary stage of the analysis.

Fit 1. We include four values of D: $D = -0.35$, -0.38, -0.4, and -0.42. We parametrize the amplitude of leading corrections to scaling by using Eq. (24). The coefficients of corrections related to the analytic background of the magnetic susceptibility are approximated by a linear function of D. All other coefficients of subleading corrections are assumed to be constant.

Let us summarize the free parameters of the fit: K_c for each value of D, R_i^* for each dimensionless quantity D^*, a_i [Eq. (24)], for each dimensionless quantity c [Eq. (24)], two coefficients for each of U_4, U_6, and ξ_{2nd}/L for the correction related to the analytic background of the magnetic susceptibility, one coefficient for the second subleading correction of ξ_{2nd}/L, and one coefficient for probing a possible correction $\propto L^{-2.022\,665}$ in Z_a/Z_p.

Fit 2. We use the same *Ansatz* as for fit 1. In contrast to fit 1, we include all six values of D, where we simulated at.

Fit 3. We use the same data set as for fit 2. We use the same approximations for the coefficients in Eq. (22) as in fits 1 and 2. In contrast to fits 1 and 2, we add an additional correction term $e_i L^{-\epsilon_3}$, where now ϵ_3 is a free parameter of the fit. It is assumed to be the same for all four dimensionless quantities. In the *Ansatz*, e_i does not depend on D.

In our fits, we include all data with a linear lattice size $L \geqslant L_{\min}$. Since corrections decrease with increasing L, the fits should become better, up to statistical fluctuations, with increasing $L_{\min}$. In the following, we always plot results of the fits versus the minimal lattice size $L_{\min}$. Let us discuss the results of the fits in detail.

In the case of fit 1 we get $\chi^2/\text{DOF} = 4.68$, 1.73, 1.22, and 1.01 for $L_{\min} = 6$, 7, 8, and 9, respectively. For $L_{\min} \geqslant 10$ we get χ^2/DOF slightly smaller than one. The numbers for fit 2 look similar: We get $\chi^2/\text{DOF} = 4.54$, 1.68, 1.22, and 1.02 for $L_{\min} = 6$, 7, 8, and 9, respectively. Again, for $L_{\min} \geqslant 10$ we get χ^2/DOF slightly smaller than one. In the case of fit 3, we get $\chi^2/\text{DOF} = 1.04$ for $L_{\min} = 6$. For $L_{\min} \geqslant 7$ we get χ^2/DOF slightly smaller than one.

In the case of fit 3 we get $\epsilon_3 \approx 5$, where the error bar is smaller than 1 only for $L_{\min} \leqslant 9$. We should be cautious in interpreting this result, since it is essentially based only on a few small lattice sizes that discriminate fits 2 and 3. Certainly, we can not exclude a correction with a smaller correction exponent and a small amplitude.

In the figures below we show data points for a p value $p > 0.01$ only. Corresponding to the χ^2/DOF discussed above, p gets rapidly larger than this value, with increasing $L_{\min}$.

In Fig. 3 we give our numerical results for the amplitude of the correction $\propto L^{-\omega_{NR}}$ of Z_a/Z_p. We find that it is compatible with zero. For comparison, we have reanalyzed the data of [29] for the Blume-Capel model at $q_3 = 0$ for $D = 0.641$, 0.655, and $\ln 2$. We used the final estimates of the fixed-point values of the dimensionless quantities obtained here as input, taking into account their covariances. As estimate of the amplitude of the correction $\propto L^{-\omega_{NR}}$ of Z_a/Z_p we find $d = -0.047(5)$. In the case of the other three quantities it is impossible to disentangle the correction $\propto L^{-\omega_{NR}}$ from the analytic background of the magnetization.
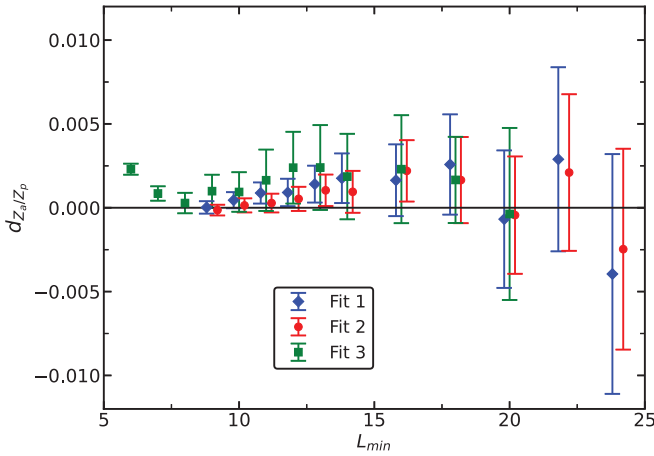
FIG. 3. Numerical estimates of the amplitude d_{Z_a/Z_p} of corrections $\propto L^{-2.022\,665}$ in Z_a/Z_p as a function of the minimal lattice size $L_{\min}$. These estimates are obtained from the fits 1, 2, and 3, which are discussed in the text. Note that the values on the x axis are slightly shifted to reduce overlap of the symbols.

In Fig. 4 we plot the estimates of $-D^*$ obtained by the three different fits as a function of $L_{\min}$. We quote as final result

$$D^* = -0.380(5). \tag{25}$$

The central value and the error bar are chosen such that for $10 \leqslant L_{\min} \leqslant 18$ the results of the three fits, including their error bars, are covered.

In Fig. 5 we plot our estimates of $(Z_a/Z_p)^*$ obtained by using fits 1, 2, and 3. The value of our final result is determined by fit 1 for $L_{\min} = 11$ up to 20. The error bar is chosen such that up to $L_{\min} = 18$ the results, including their error bars, of all three fits are covered. We quote
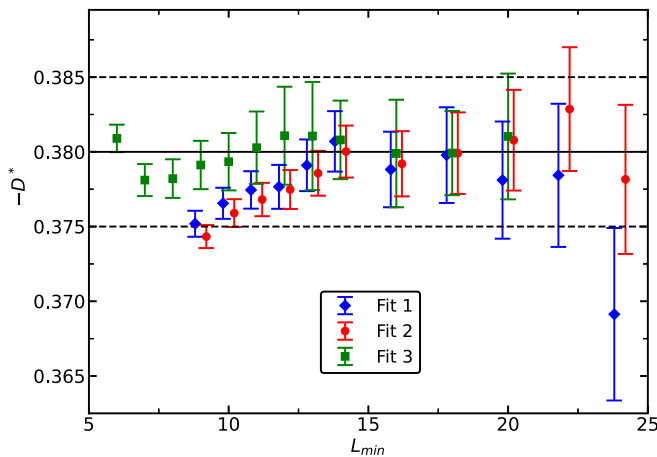
$$(Z_a/Z_p)^* = 0.542\,53(1). \tag{26}$$

FIG. 4. Estimates of $-D^*$ plotted versus the minimal lattice size $L_{\min}$ taken into account in the fit. The numerical estimates of $-D^*$ are obtained from the fits 1, 2 and 3, which are discussed in the text. The solid black line gives our final estimate of $-D^*$, while the dashed lines indicate the error bar. Note that the values on the x axis are slightly shifted to reduce overlap of the symbols.
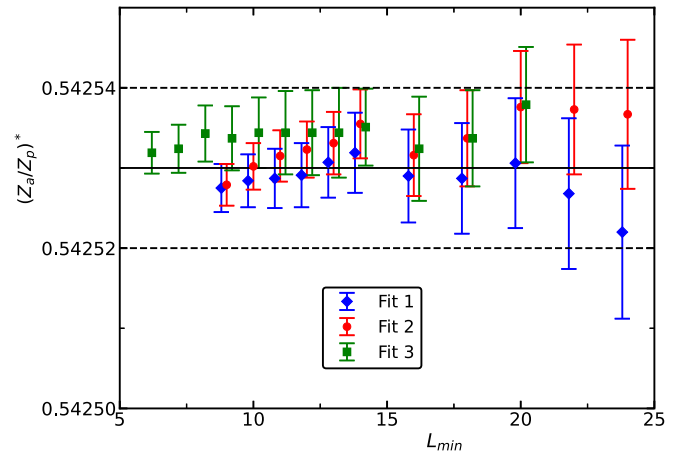

FIG. 5. Numerical estimates of $(Z_a/Z_p)^*$ obtained from the fits 1, 2 and 3, which are discussed in the text. These estimates are plotted versus the minimal lattice size $L_{\min}$ taken into account in the fit. The solid black line gives our final estimate of $(Z_a/Z_p)^*$, while the dashed lines indicate the error bar. Note that the values on the x axis are slightly shifted to reduce overlap of the symbols.

Performing a similar analysis we arrive at $U_4^* = 1.603\,59(4)$, $U_6^* = 3.105\,35(10)$, and $(\xi_{2nd}/L)^* = 0.643\,12(1)$. These numbers can be compared with $(Z_a/Z_p)^* = 0.5425(1)$, $U_4^* = 1.6036(1)$, $U_6^* = 3.1053(5)$, and $(\xi_{2nd}/L)^* = 0.6431(1)$, which were obtained in [29]. Note that in the analysis of [29] we assumed that there is a correction with the exponent $\omega' = 1.67(11)$, Ref. [20], which leads to an increase of the systematic error compared with the hypothesis that there is no such correction. Furthermore, the statistics in this study is considerably larger than that of [29]. From a finite-size scaling study of the Ising model on the simple cubic lattice the authors of Ref. [41] get $U_4^* = 1.603\,56(15)$. Note that the authors use a different definition of U_4. We have converted their numerical result correspondingly. As an example of many older results we quote $U_4^* = 1.6044(10)$ [4]. Note the authors of [4] performed a joint analysis of several different models that are supposed to share the three-dimensional Ising universality class.

Note that the fixed-point values R^* of dimensionless quantities depend on the universality class. Furthermore, one should notice that R^* depends on the global geometry of the system. The numbers quoted here are only valid for the torus geometry with $L_0 = L_1 = L_2 = L$.

TABLE V. Results for the critical coupling K_c for different values of D at $q_3 = 0.129$. For a discussion see the text.

D	K_c
-0.3	0.234765504(20)
-0.35	0.232071588(15)
-0.38	0.230514310(10)
-0.4	0.229500032(12)
-0.42	0.228504501(14)
-0.46	0.226568459(20)

Finally, in Table V we give our estimates of the critical value K_c of the coupling K. The error is estimated in a similar fashion as for the quantities discussed above.

D. U_4 and U_6 at fixed values of Z_a/Z_p or ξ_{2nd}/L

In order to get an estimate of ω and a check of the results of the previous section, we analyze, similar to previous work (see, for example, [10,13,29], U_4 and U_6 at fixed values of Z_a/Z_p or ξ_{2nd}/L. As discussed, for example, in [10], it is advantageous to fix Z_a/Z_p and ξ_{2nd}/L to good approximations of their fixed-point values, respectively. Here we take $Z_a/Z_p = 0.542\,53$ and $\xi_{2nd}/L = 0.643\,12$. The quantities behave as

$$\bar{U}_4 = \bar{U}_4^* + \bar{b}(D)L^{-\omega} + \bar{b}_2[\bar{b}(D)L^{-\omega}]^2$$
$$+ \cdots + \bar{c}(D)L^{-\epsilon} + \cdots . \qquad (27)$$

The bar on top of the quantities refers to the fact that the quantity is taken at either $Z_a/Z_p = 0.542\,53$ or $\xi_{2nd}/L = 0.643\,12$. This means that we evaluate for each lattice size L the value of K, where Z_a/Z_p or ξ_{2nd}/L assumes the desired value. Then U_4 and U_6 are evaluated at this particular value of K. For a more detailed discussion of Eq. (27), see Sec. III of Ref. [10] and references therein. In our *Ansätze* we did not use the term $\bar{b}_2[\bar{b}(D)L^{-\omega}]^2$ since $\bar{b}(D)$ is small for the values of D that we consider. The term $\bar{c}(D)L^{-\epsilon}$ represents subleading corrections.

In the case of U_4 the leading one is $c(D)L^{-2+\eta}$ due to the analytic background of the magnetic susceptibility. In addition, in the case of ξ_{2nd}/L, we expect a correction with the exponent $\epsilon_2 = 2$. The correction $L^{-\omega_{NR}}$ should be highly suppressed in our case.

We consider the two *Ansätze*

$$\bar{U}_4 = \bar{U}_4^* + \bar{b}(D)L^{-\omega} + \bar{c}_1(D)L^{-\epsilon_1} \qquad (28)$$

and

$$\bar{U}_4 = \bar{U}_4^* + \bar{b}(D)L^{-\omega} + \bar{c}_1(D)L^{-\epsilon_1} + \bar{c}_2(D)L^{-\epsilon_2}. \qquad (29)$$

We parametrized $\bar{b}(D)$ by

$$\bar{b}(D) = \bar{b}_1(D - D^*) + \frac{1}{2}\bar{b}_2(D - D^*)^2, \qquad (30)$$

where the free parameters are D^*, $\bar{b}_1$, and $\bar{b}_2$. An advantage of this parametrization is that D^* is a direct outcome of the fit. Since the values of D are contained in a narrow interval, we assumed $\bar{c}_1(D)$ and $\bar{c}_2(D)$ to be constant in the fit.

First we analyzed our data for U_4 at $Z_a/Z_p = 0.542\,53$. Here we only used *Ansatz* (28), with $\epsilon_1 = 2 - \eta$ as subleading correction exponent. Fitting data for all values of D, we get $\chi^2/\text{DOF} = 4.58, 1.30, 1.13$, and 1.08 for $L_{min} = 6, 7, 8$, and 9, respectively. Going to larger L_{min}, χ^2/DOF remains slightly larger than one.

Next, we analyzed our data for U_4 at $\xi_{2nd}/L = 0.643\,12$ by using the *Ansatz* (28) with $\epsilon_1 = 2 - \eta$. Fitting data for all values of D, we get $\chi^2/\text{DOF} = 2.72, 1.90, 1.50, 1.31, 1.11$, and 1.06, for $L_{min} = 6, 7, 8, 9, 10$, and 11, respectively. For $L_{min} \geqslant 12$, χ^2/DOF drops slightly below one.

Since for fixing $\xi_{2nd}/L = 0.643\,12$ the χ^2/DOF decreases more slowly with increasing L_{min} at small L_{min} than for fixing $Z_a/Z_p = 0.542\,53$ and also motivated by the behavior of the results for D^*, we analyzed our data for U_4 at $\xi_{2nd}/L =$
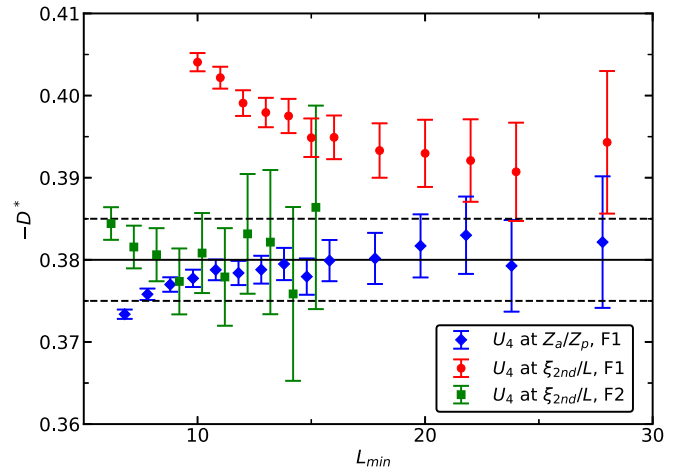

FIG. 6. We plot estimates of $-D^*$ obtained by fitting U_4 at $Z_a/Z_p = 0.542\,53$ and $\xi_{2nd}/L = 0.643\,12$ by using the *Ansatz* (28) versus the minimal lattice size L_{min} taken into account in the fit. In the legend the *Ansatz* (28) is indicated by F1. In the case of fixing $\xi_{2nd}/L = 0.643\,12$ we fitted in addition by using the *Ansatz* (29), which is indicated by F2. The solid and the dashed lines give the final result of the previous section and the corresponding error bar. Note that the values on the x axis are slightly shifted to reduce overlap of the symbols.

$0.643\,12$ in addition by using the *Ansatz* (29) with $\epsilon_1 = 2 - \eta$ and $\epsilon_2 = 2$. Here we find $\chi^2/\text{DOF} = 0.938$ already for $L_{min} = 6$. For larger values of L_{min} it stays below one.

In Fig. 6 we give our results for D^* obtained by using these three different fits. In the case of fixing $Z_a/Z_p = 0.542\,53$ the estimate is consistent with the one of the previous section, starting from $L_{min} = 8$. The situation is quite different for fixing $\xi_{2nd}/L = 0.643\,12$ and *Ansatz* (28). For small L_{min} the estimate of $-D^*$ is too large compared with the one of the previous section and only slowly decreases with increasing L_{min}. In contrast, using the *Ansatz* (29), we see consistent results, starting from very small L_{min}. We conclude that the analysis presented here confirms the final estimate of D^*, Eq. (25), given above.

Next, in Fig. 7, we plot estimates of ω obtained by these three fits. In contrast to D^*, there is very little difference between the results of the different fits. In Fig. 7, we give the estimate $\omega = 0.829\,68(23)$ of Ref. [17] for comparison. Our data are certainly consistent with this estimate. As our final estimate we might quote $\omega = 0.825(20)$. This is less precise than $\omega = 0.832(6)$ given in Ref. [29]. Note that this study was not designed for an accurate estimate of ω. To this end, a larger range of D is needed.

In order to understand better the interplay of the two corrections, we have rewritten the *Ansatz* (29) in the form

$$\bar{U}_4 = \bar{U}_4^* + \bar{b}(D)L^{-\omega} + \bar{c}(D)L^{-\epsilon_1} + \bar{d}(D)(L^{-\epsilon_1} - L^{-\epsilon_2}). \qquad (31)$$

Here we fitted with $\omega = 0.829\,68$ fixed and $\bar{c}$ and $\bar{d}$ not depending on D. Data for U_4 at $\xi_{2nd}/L = 0.643\,12$ for $D = -0.35, -0.38, -0.4$, and -0.42 are included in the fit. The estimates of the amplitudes $\bar{c}$ and $\bar{d}$ are plotted in Fig. 8. The results clearly indicate that there are two different
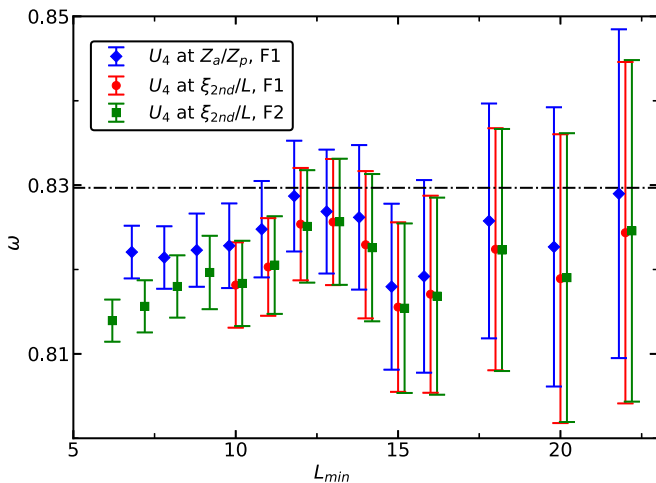
FIG. 7. We plot estimates of ω obtained by fitting U_4 at $Z_a/Z_p = 0.542\,53$ and $\xi_{2nd}/L = 0.643\,12$ by using the *Ansatz* (28) versus the minimal lattice size L_{min} taken into account in the fit. In the legend the *Ansatz* (28) is indicated by F1. In the case of fixing $\xi_{2nd}/L = 0.643\,12$ we fitted in addition by using the *Ansatz* (29), which is indicated by F2. Note that the values on the x axis are slightly shifted to reduce overlap of the symbols. The dashed-dotted line gives the result of Ref. [17].

corrections with exponents $\epsilon \approx 2$. Furthermore, the fact that $|\bar{d}|$ being clearly larger than $|\bar{c}|$ shows that at least for the lattice sizes L considered here, the corrections numerically cancel to a considerable extent. Just to give an idea, for example $10^{-\eta} = 0.9198\ldots$ or $100^{-\eta} = 0.8460\ldots$, using the CB estimate $\eta = 0.036\,297\,8$ [17,47]. This fact might explain the behavior of the results for $-D^*$ obtained by fitting U_4 at $\xi_{2nd}/L = 0.643\,12$ with the *Ansatz* (28). We also analyzed U_6
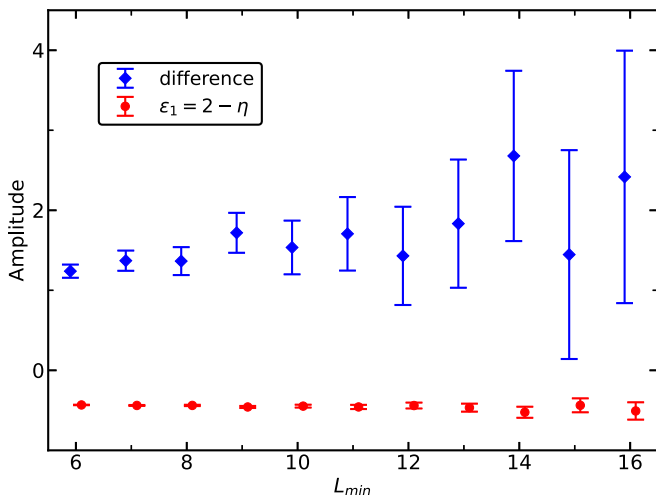

FIG. 8. We plot estimates of amplitudes of subleading corrections obtained by fitting U_4 at $\xi_{2nd}/L = 0.643\,12$ by using the *Ansatz* (31) versus the minimal lattice size L_{min} taken into account in the fit. We give the amplitude $\bar{c}$ of $L^{-\epsilon_1}$ and $\bar{d}$ of the difference $L^{-\epsilon_1} - L^{-\epsilon_2}$. In the legend we give either the value of the correction exponent ϵ_1 or "difference." Note that the values on the x axis are slightly shifted to reduce overlap of the symbols.

at fixed values of Z_a/Z_p or ξ_{2nd}/L. Since the results are very similar to those for U_4, we abstain from a discussion.

Finally, we have reanalyzed our data for the standard Ising model obtained in Ref. [29]. We determined the amplitude $\bar{b}$ of the leading correction in U_4 at $Z_a/Z_p = 0.542\,53$ using $\omega = 0.829\,68$ as input. Combining the result $\bar{b}_{Ising} \approx -0.2$ of this analysis with the data obtained here for the derivative of the amplitude of the leading correction with respect to D at $D = -0.38$, we conclude that at $D = -0.38$, for $q_3 = 0.129$, leading corrections to scaling are suppressed at least by a factor of about 270 compared with the standard Ising model on the simple cubic lattice.

E. Magnetic susceptibility

In order to determine the critical exponent η, we analyze the magnetic susceptibility χ at $Z_a/Z_p = 0.542\,53$ or $\xi_{2nd}/L = 0.643\,12$. Fixing Z_a/Z_p, no additional corrections with $\epsilon \approx 2$ are introduced. For ξ_{2nd}/L fixed, the statistical error is smaller. However, the analysis of the data is more difficult due to subleading corrections with the exponent $\epsilon_2 = 2$.

In addition to the magnetic susceptibility $\bar{\chi}$ at a fixed value of a dimensionless quantity, we analyzed the improved version of it

$$\bar{\chi}_{imp} = \bar{\chi}\bar{U}_4^x, \tag{32}$$

where the bar indicates that the quantity is taken at a fixed value of Z_a/Z_p or ξ_{2nd}/L. The exponent x is tuned such that leading corrections to scaling are eliminated. For simplicity, we took the result obtained in Sec. VII of Ref. [29]: $x = -0.66$ and $x = -0.57$ for fixing Z_a/Z_p and ξ_{2nd}/L, respectively.

We fit our data for fixing Z_a/Z_p and ξ_{2nd}/L with the *Ansatz*

$$\bar{\chi} = \bar{c}L^{2-\eta} + \bar{b}. \tag{33}$$

In the case of fixing ξ_{2nd}/L we used in addition

$$\bar{\chi} = \bar{c}L^{2-\eta}\left(1 + \bar{d}L^{-2}\right) + \bar{b}. \tag{34}$$

Our results for $D = -0.38$ and the standard version of $\bar{\chi}$ are given in Fig. 9. In the case of fixing Z_a/Z_p, χ^2/DOF already drops below one at $L_{min} = 9$. In contrast, for fixing ξ_{2nd}/L it drops below two at $L_{min} = 16$ and remains larger than 1.5 even for larger L_{min}. Using the *Ansatz* (34) we get $\chi^2/\text{DOF} = 1.23$ for $L_{min} = 6$, corresponding to $p = 0.16$. The χ^2/DOF stays roughly at this level going to larger values of L_{min}. One might be tempted to take $\eta = 0.036\,299(8)$ obtained from the fit using the *Ansatz* (33) of χ at $Z_a/Z_p = 0.542\,53$ with $L_{min} = 10$ as final result, where $\chi^2/\text{DOF} = 0.93$ corresponding to $p = 0.58$.

Nevertheless, as our final estimate we quote the more cautious

$$\eta = 0.036\,284(40)\,. \tag{35}$$

It is chosen such that it covers the results, including their error bars, obtained by fitting χ at $Z_a/Z_p = 0.542\,53$ by using the *Ansatz* (33) up to $L_{min} = 26$. In addition the results, including their error bars, obtained by fitting χ at $\xi_{2nd}/L = 0.643\,12$ by using the *Ansatz* (33) for $L_{min} = 22$ and 24 are covered. In the case of fitting χ at $\xi_{2nd}/L = 0.643\,12$ by using the *Ansatz*
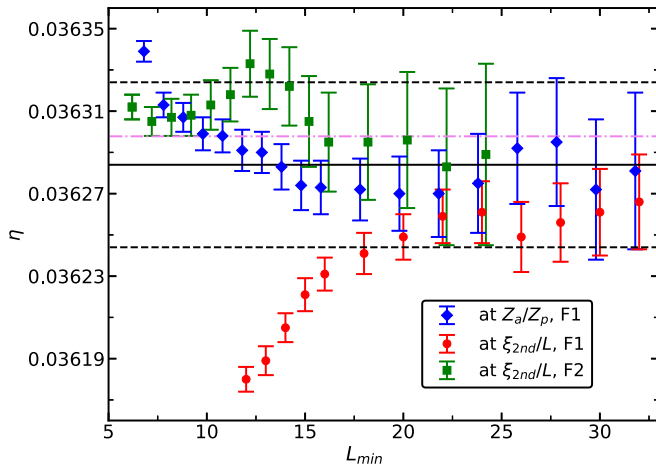
FIG. 9. Numerical estimates of η for $D = -0.38$ plotted versus the minimal lattice size $L_{\min}$ taken into account in the fit. We have fitted the nonimproved χ by using the *Ansatz* (33) for both fixing Z_a/Z_p and ξ_{2nd}/L. These fits are denoted by F1 in the legend. In the case of fixing ξ_{2nd}/L, we give results obtained by using the *Ansatz* (34) in addition. These fits are denoted by F2 in the legend. The values on the x axis are slightly shifted to reduce overlap of the symbols. The solid black line gives our final estimate of η, while the dashed lines indicate the error bar. The dashed-dotted line gives the estimate of Refs. [17,47]. Note that the error bar of the CB result is by a factor of 20 smaller than the one obtained here.

(34) the results, including their error bars, are covered for the majority of $L_{\min}$ values with $L_{\min} \leqslant 22$.

Finally, we study the effect of deviations of D from D^*. To this end we have fitted χ at $Z_a/Z_p = 0.54253$ and its improved version for all values of D we simulated at by using the *Ansatz* (33). Our results for $L_{\min} = 12$ are given in Fig. 10. We see that the estimate of η obtained from $\bar{\chi}$ has a clear
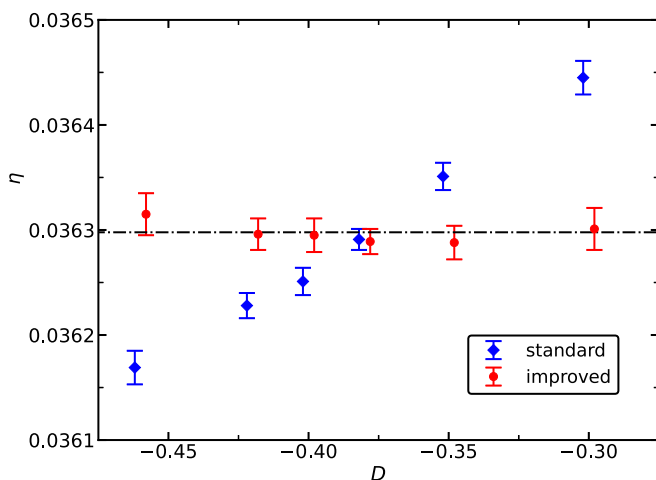

FIG. 10. Numerical estimates of η obtained by fitting χ at $Z_a/Z_p = 0.54253$ by using the *Ansatz* (33) versus D. We compare results obtained for the standard and the improved, Eq. (32), version of the magnetic susceptibility. In all cases we give the estimate obtained with $L_{\min} = 12$. The values on the x axis are slightly shifted to reduce overlap of the symbols. The dashed-dotted line gives the estimate of Refs. [17,47].
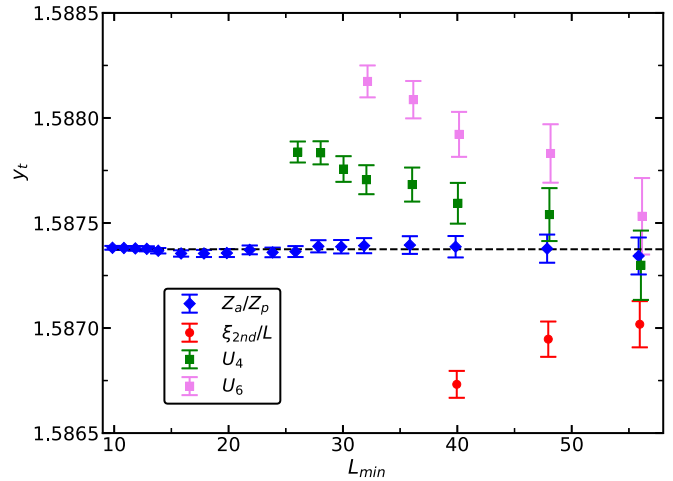

FIG. 11. Numerical estimates of y_t for $D = -0.38$ obtained by fitting the slopes of dimensionless quantities at $Z_a/Z_p = 0.54253$ by using the *Ansatz* (36) versus the minimal lattice size $L_{\min}$ that is taken into account. The dashed-dotted line gives the estimate of Refs. [17,47]. The legend refers to the quantity that is analyzed.

dependence on D. In contrast, this dependence is, within errors, eliminated for $\bar{\chi}_{\text{imp}}$. This finding confirms that the exponent x is universal. Note that in Ref. [29], we have determined x by studying the Blume-Capel model at $q_3 = 0$. Furthermore, we see that for $D = -0.38$ the estimates obtained by fitting $\bar{\chi}$ and $\bar{\chi}_{\text{imp}}$ essentially coincide. This confirms our result $D^* = -0.380(5)$, Eq. (25), obtained above. Furthermore, no revision of our final estimate (35) is needed.

F. The exponent ν

We study the slopes of dimensionless quantities at a fixed value of a dimensionless quantity. Below we restrict the discussion on fixing $Z_a/Z_p = 0.54253$ since Z_a/Z_p has virtually no corrections $\propto L^{-\epsilon}$, where $\epsilon \approx 2$.

1. Analyzing quantity by quantity

In this section we have fitted the slopes of dimensionless quantities one by one. First we have fitted the data for $D = -0.38$ with the *Ansatz*

$$\bar{S}_R = \bar{a} L^{y_t}, \tag{36}$$

not taking into account corrections. The estimates of y_t obtained this way are given in Fig. 11. In the figure we give only results that correspond to $p > 0.01$. For the slope of Z_a/Z_p, actually already for $L_{\min} = 10$, we get $\chi^2/\text{DOF} = 0.96$ corresponding to $p = 0.52$. Furthermore, we see that for the slope of Z_a/Z_p the estimate of y_t does change little with increasing $L_{\min}$. For $L_{\min} = 10$ we get $y_t = 1.587382(9)$, consistent with the CB estimate $y_t = 1.587375(10)$ [17,47].

In the case of the other quantities, we see a clear dependence of the estimate on $L_{\min}$. At least, in all cases the CB estimate is approached as $L_{\min}$ increases. This observation is consistent with the fact that only in the case of the slope of Z_a/Z_p we do not expect corrections $\propto L^{-\epsilon}$ with $\epsilon \approx 2$.
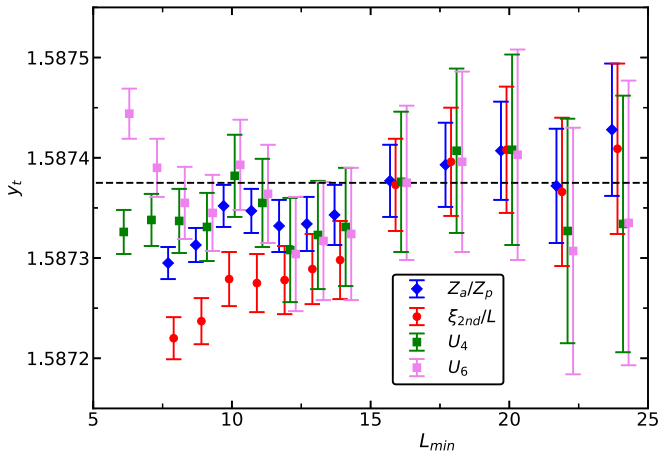
FIG. 12. Numerical estimates of y_t for $D = -0.38$ obtained by fitting the slopes of dimensionless quantities with the *Ansatz* (37) versus the minimal lattice size $L_{\min}$ that is taken into account. The dashed-dotted line gives the estimate of Refs. [17,47]. The legend refers to the quantity that is analyzed in the fit.

Next, in Fig. 12 we give estimates of y_t obtained by fitting with the *Ansatz*

$$\bar{S}_R = \bar{a}L^{y_t}\left(1 + \bar{c}L^{-\epsilon}\right), \tag{37}$$

where $\epsilon = 2 - \eta$. Here $p > 0.01$ is reached for much smaller $L_{\min}$ than for *Ansatz* (36). Furthermore, the estimates obtained by analyzing the different slopes are close to each other starting from small values of $L_{\min}$. For example, for $L_{\min} = 14$ the preliminary result $y_t = 1.58733(7)$ corresponding to $\nu = 0.629989(28)$ covers the estimates obtained by analyzing the four different quantities. It is fully consistent with the estimate of Refs. [17,47]. Note that for $L_{\min} = 14$ we get $\chi^2/\text{DOF} = 0.96$, 1.34, 1.18, and 1.26 corresponding to $p = 0.51$, 0.12, 0.25, and 0.17 for the slopes of Z_a/Z_p, ξ_{2nd}, U_4, and U_6, respectively.

Next, we focus on the slope of Z_a/Z_p. It should not contain a correction related to the analytic background and the contribution $\propto L^{-\omega_{NR}}$ should be very small. One expects a correction with the correction exponent $y_t + \omega$. For a discussion see, for example, Sec. III of Ref. [10]. It turns out that replacing $\epsilon = 2 - \eta$ by $\epsilon = y_t + \omega \approx 2.417055$ in the *Ansatz* (37) the numerical estimates of y_t change only slightly. This can be explained by the fact that the amplitude of the correction is small.

In Fig. 13 we give estimates of y_t obtained by fitting the slope of Z_a/Z_p with the *Ansatz* (37) and setting the correction exponent to $\epsilon = y_t + \omega$. We give data for $D = -0.35$, -0.38, -0.4, and -0.42. We see only a small variation of the result with D. Here we take $y_t = 1.58734(4)$ corresponding to $\nu = 0.629985(16)$ as preliminary result that covers estimates obtained for $10 \leqslant L_{\min} \leqslant 14$ for $D = -0.38$. Note that $\chi^2/\text{DOF} = 0.91$ corresponding to $p = 0.61$ for $L_{\min} = 10$.

2. Joint fit using all four dimensionless quantities

Finally, we performed joint fits of the slopes of all four dimensionless quantities using the *Ansatz* (37) and in addition

$$\bar{S}_R = \bar{a}L^{y_t}\left(1 + \bar{c}_1 L^{-\epsilon_1} + \bar{c}_2 L^{-\epsilon_2} + c_3 L^{-\epsilon_3}\right), \tag{38}$$
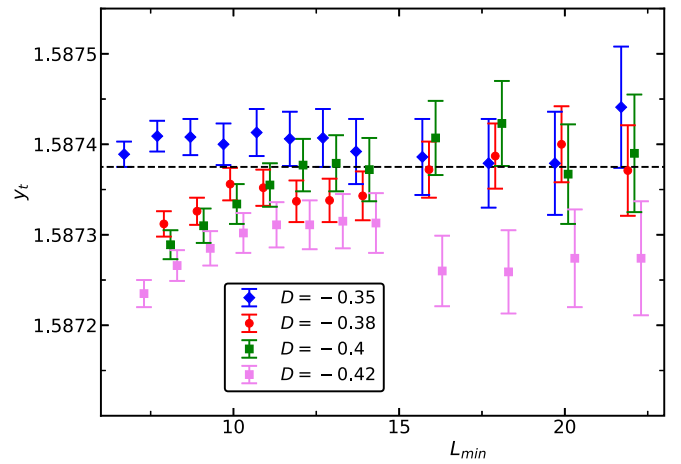

FIG. 13. Numerical estimates of y_t for $D = -0.35, -0.38, -0.4$, and -0.42 obtained by fitting the slope of Z_a/Z_p by using the *Ansatz* (37) with $\epsilon = y_t + \omega$ as correction exponent. These estimates are plotted versus the minimal lattice size $L_{\min}$ taken into account in the fit. Note that the values on the x axis are slightly shifted to reduce overlap of the symbols. The dashed-dotted line gives the estimate of Refs. [17,47].

where $\epsilon_1 = 2 - \eta$, $\epsilon_2 = 2$, and $\epsilon_3 = y_t + \omega$. We set $\bar{c}_1 = 0$ for the slope of Z_a/Z_p and $\bar{c}_2 = 0$ for the slopes of Z_a/Z_p, U_4, and U_6. In Fig. 14 we give the results for y_t obtained by performing these fits using our data for $D = -0.38$. It turns out that for the *Ansatz* (38) an acceptable χ^2/DOF is reached for considerably smaller $L_{\min}$ than for *Ansatz* (37). On the other hand, the estimates obtained for y_t are similar. As our preliminary result we quote

$$y_t = 1.58739(7) \tag{39}$$

corresponding to $\nu = 0.629965(28)$. It covers the estimates obtained by both *Ansätze* (37) and (38), for $16 \leqslant L_{\min} \leqslant 22$.
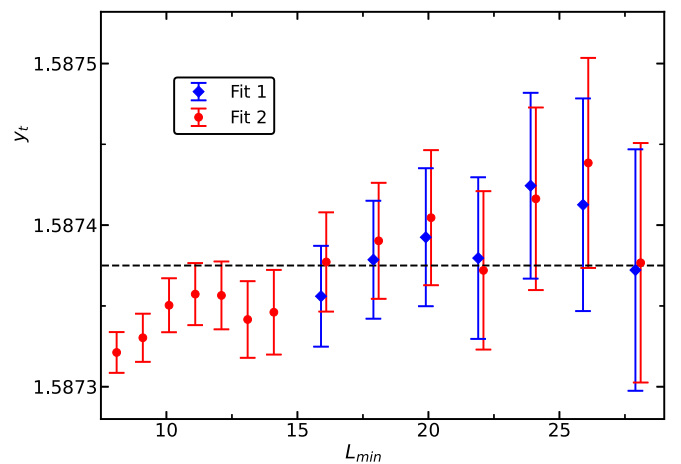

FIG. 14. Numerical estimates of y_t for $D = -0.38$ obtained by fitting the slopes of all four dimensionless quantities jointly with the *Ansatz* (37) or *Ansatz* (38). These estimates are plotted versus the minimal lattice size $L_{\min}$ that is taken into account in the fit. In the legend, these *Ansätze* are denoted by fit 1 and fit 2, respectively. Note that the values on the x axis are slightly shifted to reduce overlap of the symbols.
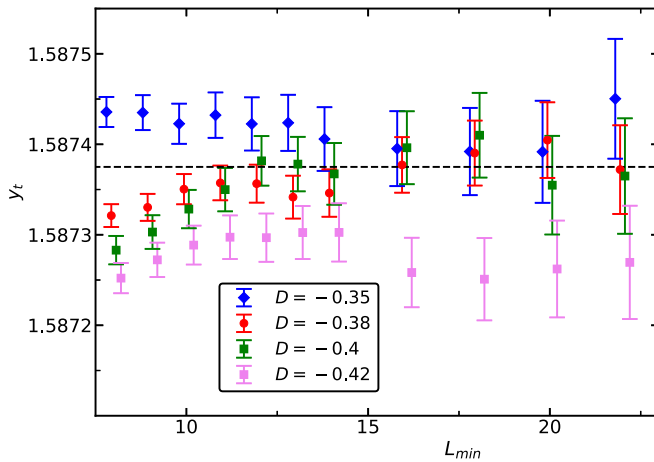
FIG. 15. Numerical estimates of y_t for $D = -0.35, -0.38, -0.4$, and -0.42 obtained by fitting the slopes of all four dimensionless quantities jointly with the *Ansatz* (38) versus the minimal lattice size $L_{\min}$ taken into account. Note that the values on the x axis are slightly shifted to reduce overlap of the symbols for different values of D.

Note that for $L_{\min} = 16$, we get $\chi^2/\mathrm{DOF} = 1.19$ and 1.14, corresponding to $p = 0.11$ and 0.17 for the *Ansätze* (37) and (38), respectively.

Finally, in Fig. 15 we give results obtained by fitting the data for $D = -0.35, -0.38, -0.4$, and -0.42 using the *Ansatz* (38). The estimates obtained for different values of D differ only by little. Hence, the estimate, Eq. (39), quoted above needs not to be revised. Similar to Eq. (32), improved slopes can be constructed. Since the dependence of our estimate of y_t on D is relatively small, we abstained from analyzing improved slopes here.

In this section we obtained three preliminary estimates of $y_t = 1/\nu$ by analyzing the slopes of dimensionless quantities in different ways. Our final result

$$\nu = 0.629\,98(5) \tag{40}$$

covers these preliminary estimates, including their error bars.

VI. SUMMARY AND OUTLOOK

We have studied a generalized Blume-Capel model on the simple cubic lattice. In addition to the nearest-neighbor coupling K_1 there is a third-nearest-neighbor coupling K_3. This model has been studied for example in Ref. [4]. Here we are aiming at the elimination of both the leading contribution to the spatial anisotropy and the leading correction to scaling. This is achieved by tuning the ratio $q_3 = K_3/K_1$ and the parameter D that controls the distribution of the spin at a given site. For the precise definition of the reduced Hamiltonian, see Sec. II. The values, where these corrections are eliminated, are denoted by q_3^{iso} and D^*. It is conjectured and numerically confirmed that the spatial anisotropy depends little on D. Hence, q_3^{iso} depends little on D. In contrast, the leading correction to scaling depends on q_3 and D in a similar strength.

In order to quantify the spatial anisotropy, we determine the correlation length in three different spatial directions in the high-temperature phase of the model. We tune q_3 such that these three correlation lengths are the same. For our final

estimate $q_3^{\mathrm{iso}} = 0.129(1)$, we determine $D^*(q_3 = 0.129) = -0.380(5)$ by using a finite-size scaling analysis similar to that of [10,13] and references therein. In addition, we obtain accurate estimates of the fixed-point values of dimensionless quantities and critical temperatures. Furthermore, the finite-size scaling analysis provides accurate estimates of the critical exponents ν and η.

In Table VI we compare these with selected results obtained by using different methods. For a more complete summary of theoretical results given in the literature, see Tables 3, 4, 5, and 6 of Ref. [25] and the references given in Table VI for more recent work. A summary of experimental estimates is given in Table 7 of Ref. [25]. In general, we find a good agreement of the results obtained by the different methods. In the cases [32,48], where the estimates are slightly out of the error bars, it is plausible that these were underestimated, rather than that there is a fundamental problem. In Ref. [50] the Blume-Capel model at $D = 0.655$ at the critical point has been studied with slab geometry and Dirichlet boundary conditions. From the behavior of the magnetization as a function of the distance from the boundary the authors obtain $\eta = 0.036\,284(16)$. One should note that, for example, the uncertainty of D^* and of the critical coupling K_c is not taken into account in the error bar that is quoted. The results of this study are fully consistent with those of the CB method. Our error bars are by a factor of 12.5 and 20 larger than those of the CB method for the exponents ν and η, respectively. Nevertheless, one should regard this study as a valuable consistency check since the approaches are complementary.

This study gives strong support to the fact that only the breaking of the spatial isotropy by the lattice gives rise to a scaling field associated with a correction exponent ≈ 2. In particular, $\omega' = 1.67(11)$ obtained by the scaling field method [20] seems to be an artifact of the method. In addition to these corrections, corrections that are intrinsic to the observable need to be taken into account, for example, the analytic background in the magnetic susceptibility.

In the model studied here, corrections to scaling are highly suppressed. Compared with the standard Ising model on the simple cubic lattice, the leading correction to isotropy is reduced by at least a factor of 180 and the leading correction to scaling at least by a factor of 270. Still the model is relatively simple to implement and can be efficiently simulated. Hence, it might be the model of choice to study universal properties of the Ising universality class, for example, interfacial properties, boundary critical phenomena, or dynamics.

Unfortunately, the idea of this work can not be directly adopted for $O(N)$-symmetric models with $N > 1$ as we discuss in Appendix B.

APPENDIX A: RANDOM NUMBER GENERATORS

Motivated by the discussion, Ref. [51] and references therein, on the reliability of the Mersenne Twister algorithm

TABLE VI. Selected theoretical results for critical exponents for the three-dimensional Ising universality class taken from the literature. In the first column we indicate the method that has been used. It follows the year of the publication and the reference. The most accurate results are provided by the conformal bootstrap (CB) method. Next, we give results obtained by studies of lattice models, where either high-temperature series expansions (HT) or Monte Carlo (MC) simulations are used. In some of the studies a number of different models have been studied. This is indicated by "var." In others, the study is either restricted to the Blume-Capel (BC) or the Ising model. Finally, we give two recent studies using the ϵ expansion and the functional renormalization group (FRG) method.

Method	Year	Ref.	ν	η	ω
CB	2016	[17,47]	0.6299709(40)	0.0362978(20)	0.82968(23)
HT, var	2002	[18]	0.63012(16)	0.03639(15)	0.825(50)
MC, var	2003	[32]	0.63020(12)	0.0368(2)	0.821(5)
MC, BC	2010	[29]	0.63002(10)	0.03627(10)	0.832(6)
MC, Ising	2018	[41]	0.629912(86)	0.03610(45)	
MC, BC, iso	2021	This work	0.62998(5)	0.036284(40)	0.825(20)
ϵ exp.	2017	[48]	0.6292(5)	0.0362(6)	0.820(7)
FRG	2020	[49]	0.63012(16)	0.0361(11)	0.832(14)

[42] we performed some runs with other generators to check the consistency of the results obtained by different generators.

In particular, we used the double precision version of Lüscher's RANLUX generator [46] at the highest luxury level. Here we made use of Lüscher's most recent implementation ranlux-3.4 taken from [52]. Note that there are a number of alternative implementations. Just search the internet with your favorite search engine.

Furthermore, we used a generator that is based on the KISS generator proposed by Marsaglia. It combines three different generators as

$$r = (r_1 + r_2 + r_3) \mod 2^{64}, \qquad (A1)$$

where $r_1, r_2, r_3 \in \{0, 1, 2, \dots, 2^{64} - 1\}$ are generated by three different, relatively simple generators. The rough idea of such a combination is that the generators compensate each other's weaknesses. For a critical discussion of the KISS generator, see Ref. [53]. Our starting point is the 64-bit implementation given in the German version of [54].

Here, we replaced the generators r_1 and r_2 by ones that are of better quality than those used in Marsaglia's original generator. For r_1 we used xoshiro256+ taken from [55]. For a discussion of the generator see [56]. As second generator we used a 96-bit linear congruential generator with the multiplier and the increment $a = c =$0xc580cadd754f7336d2eaa27d and the modulus $m = 2^{96}$ suggested by O'Neill [57]. In this case we used our own implementation. In Eq. (A1) we use the upper 64 bits.

Note that in the context of our simulations, the importance of the quality of the random bits is decreasing from high to low since the random numbers, normalized to the interval [0,1], are used for comparisons with double-precision floating point numbers. It is plausible that both the generators r_1 and r_2 would do the job on their own, which we, however, did not check here. We performed a few basic tests of the combined generator. In particular, we did run the big crush test [58] several times, with different initializations of the generator, on the upper, the middle, and lower 32 bits of the generator. These tests were passed.

The choice of the particular generator discussed here is essentially *ad hoc* and unfortunately not based on deep insight.

While we are confident that the generator is a good choice for our purpose, we do not recommend it for general use since there are certainly better tested and motivated generators that consume less CPU time.

For $D = -0.38$ we have simulated the lattice sizes $L = 12$ and 120 close to criticality with roughly equal statistics using the three choices of the random number generator. We get consistent results for the three different choices.

The bulk of the simulations have been performed either by using the SFMT or the modified KISS generator. Which generator was used is essentially determined by the history of our simulations. At a certain stage we switched from the SFMT to the modified KISS generator. As a result, the simulations for $D = -0.3, -0.35, -0.4$, were mainly performed by using the SFMT generator, while those for $D = -42$ and -0.46 were mainly performed by using the modified KISS generator. In the case of $D = -0.38$ both generators have been used on roughly the same footing. The fact that fits that include both sets of simulations give reasonable p values gives us further assurance that there is nothing terribly wrong with the generators that we have used.

To give the reader an impression on the relative performance of the generators we give the CPU time needed on one core of an Intel(R) Xeon(R) CPU E3-1225 v3 for one update and measurement cycle for $L = 32$. The program has been compiled with the gcc version 9.3.0 and the $-$O2 optimization. We need 0.00198 s, 0.00197 s, 0.00228 s, and 0.00307 s using the SFMT, the xoshiro256+, the modified KISS, and the RANLUX generator, respectively. Note that for one sweep with the local update we need exactly $L^3 = 32\,768$ random numbers. For the cluster algorithms on average about 77 200 random numbers are used in one cycle with $L/4 = 8$ single cluster and one wall-cluster update. In a simple program that only calls the random number generator, the xoshiro256+ and the modified KISS, for example, take 8×10^{-10} and 2×10^{-9} seconds per call, respectively. The difference between these numbers does not fully explain the difference in the timings for the whole measurement and update cycle given above. This might be explained by the fact that the random number generator is inlined in the code, and the result of the optimization performed by the compiler depends much on the code that is inlined.

APPENDIX B: THREE-DIMENSIONAL XY MODEL WITH NEXT-TO-NEXT-TO-NEAREST-NEIGHBOR COUPLINGS

We performed a preliminary finite-size scaling study of the XY model on the simple cubic lattice with next-to-next-to-nearest-neighbor couplings in addition to the nearest-neighbor one. The reduced Hamiltonian is given by

$$H = -K_1 \sum_{\langle xy \rangle} \vec{s}_x \vec{s}_y - K_3 \sum_{[xy]} \vec{s}_x \vec{s}_y, \qquad (B1)$$

where $\vec{s}_x$ is a unit vector with two real components. Otherwise, the notation is the same as in Sec.. II. The simulations were actually performed prior to the study discussed in the main part of this paper. Therefore, the setup slightly differs from that of the main part of this paper. In particular, we varied K_1, while keeping K_3 fixed. For $K_3 = 0.03$ and 0.05 we simulated the linear lattices $L = 8, 10, 12, ..., 20$. For $K_3 = 0.04$, we simulated $L = 6, 7, 8, ..., 20, 22, 24, ..., 30, 34, 40, 50, ..., 80$. We performed 3×10^9 measurements for $L \leqslant 20$. In the case of $K_3 = 0.04$, the number of measurements is decreasing, going to larger lattice sizes. For $L = 80$, 5.5×10^8 measurements were performed. We simulated at good estimates of the critical coupling $K_{1,c}$. These estimates were iteratively improved with increasing lattice size. Making use of $(Z_a/Z_p)^* = 0.320\,37(6)$

for the three-dimensional XY universality class [10], we get $K_{1,c} = 0.393\,164\,7(10)$, $0.373\,600\,5(2)$, and $0.354\,428\,2(10)$, for $K_3 = 0.03$, 0.04, and 0.05, respectively.

Next, we analyzed U_4 at $(Z_a/Z_p)^* = 0.320\,37$ by using the *Ansatz*

$$\bar{U}_4 = \bar{U}_4^* + \bar{b}(K_3)L^{-\omega} + \bar{c}(K_3)L^{-2+\eta}, \qquad (B2)$$

using the estimates $U_4^* = 1.242\,96(8)$ and $\omega = 0.789(4)$ for the three-dimensional XY universality class [10]. For $\omega = 0.789$ fixed, we arrive at $\bar{b} = -0.031(2)$, $-0.0045(15)$, and $0.021(2)$ for $K_3 = 0.03$, 0.04, and 0.05, respectively. The error of $\bar{b}$ is dominated by the uncertainty of U_4^* that we used as input. Linearly interpolating, we arrive at $q_3^* = 0.113(2)$. In the large-N limit, where N counts the number of components of the spin $\vec{s}_x$, $q_{3,N=\infty}^{\mathrm{iso}} = q_{3,\mathrm{free}}^{\mathrm{iso}} = 0.125$. Therefore, it is plausible that $0.125 < q_{3,\mathrm{XY}}^{\mathrm{iso}} < q_{3,\mathrm{Ising}}^{\mathrm{iso}}$, meaning that $q_3^{\mathrm{iso}} > q_3^*$ for the XY model. Hence, following the argument of Sec. II, we can not find a model similar to Eq. (1), where both the leading correction to scaling and the leading violation of isotropy are eliminated. Still the XY model at q_3^* might be useful since the spatial anisotropy should be considerably reduced compared with $q_3 = 0$.

[1] J. H. Chen, M. E. Fisher, and B. G. Nickel, Unbiased Estimation of Corrections to Scaling by Partial Differential Approximants, Phys. Rev. Lett. **48**, 630 (1982).

[2] M. E. Fisher and J. H. Chen, The validity of hyperscaling in three dimensions for scalar spin systems, J. Phys. (Paris) **46**, 1645 (1985).

[3] M. N. Barber, Finite-size Scaling, in *Phase Transitions and Critical Phenomena*, edited by C. Domb and J. L. Lebowitz, Vol. 8 (Academic, New York, 1983).

[4] H. W. J. Blöte, E. Luijten, and J. R. Heringa, Ising universality in three Dimensions: a Monte Carlo study, J. Phys. A: Math. Gen. **28**, 6289 (1995).

[5] H. G. Ballesteros, L. A. Fernández, V. Martín-Mayor, and A. Muñoz Sudupe, Finite Size Scaling and "perfect" actions: the three dimensional Ising model, Phys. Lett. B **441**, 330 (1998).

[6] M. Hasenbusch, K. Pinn, and S. Vinti, Critical exponents of the three-dimensional Ising universality class from finite size scaling with standard and improved actions, Phys. Rev. B **59**, 11471 (1999).

[7] M. Hasenbusch and T. Török, High precision Monte Carlo study of the 3D XY-universality class, J. Phys. A: Math. Gen. **32**, 6361 (1999).

[8] M. Campostrini, M. Hasenbusch, A. Pelissetto, P. Rossi, and E. Vicari, Critical behavior of the three-dimensional XY universality class, Phys. Rev. B **63**, 214503 (2001).

[9] M. Campostrini, M. Hasenbusch, A. Pelissetto, and E. Vicari, Theoretical estimates of the critical exponents of the superfluid transition in ⁴He by lattice methods, Phys. Rev. B **74**, 144506 (2006).

[10] M. Hasenbusch, Monte Carlo study of an improved clock model in three dimensions, Phys. Rev. B **100**, 224517 (2019).

[11] M. Hasenbusch, Eliminating leading corrections to scaling in the 3-dimensional $O(N)$-symmetric ϕ^4 model: $N = 3$ and 4, J. Phys. A: Math. Gen. **34**, 8221 (2001).

[12] M. Campostrini, M. Hasenbusch, A. Pelissetto, P. Rossi, and E. Vicari, Critical exponents and equation of state of the three-dimensional Heisenberg universality class, Phys. Rev. B **65**, 144520 (2002).

[13] M. Hasenbusch, Monte Carlo study of a generalized icosahedral model on the simple cubic lattice, Phys. Rev. B **102**, 024406 (2020).

[14] M. Hasenbusch, F. Parisen Toldin, A. Pelissetto, and E. Vicari, Universality class of 3D site-diluted and bond-diluted Ising systems, J. Stat. Mech.: Theory Exp. (2007) P02016.

[15] K. Symanzik, Continuum limit and improved action in lattice theories: (I). Principles and ϕ^4 theory, Nucl. Phys. B **226**, 187 (1983); Continuum limit and improved action in lattice theories: (II). O(N) non-linear sigma model in perturbation theory, **226**, 205 (1983).

[16] D. Poland, S. Rychkov, and A. Vichi, The conformal bootstrap: Theory, numerical techniques, and applications, Rev. Mod. Phys. **91**, 015002 (2019).

[17] D. Simmons-Duffin, The lightcone bootstrap and the spectrum of the 3d Ising CFT, J. High Energy Phys. 03 (2017) 086.

[18] M. Campostrini, A. Pelissetto, P. Rossi, and E. Vicari, 25th-order high-temperature expansion results for three-dimensional Ising-like systems on the simple-cubic lattice, Phys. Rev. E **65**, 066127 (2002).

[19] M. Campostrini, A. Pelissetto, P. Rossi, and E. Vicari, Two-point correlation function of three-dimensional O(N) models: The critical limit and anisotropy, Phys. Rev. E **57**, 184 (1998).

[20] K. E. Newman and E. K. Riedel, Critical exponents by the scaling-field method: The isotropic N-vector model in three dimensions, Phys. Rev. B **30**, 6615 (1984).

[21] D. F. Litim and L. Vergara, Subleading critical exponents from the renormalization group, Phys. Lett. B **581**, 263 (2004).

[22] M. Hasenbusch, Two- and three-point functions at criticality: Monte Carlo simulations of the improved three-dimensional Blume-Capel model, Phys. Rev. E **97**, 012119 (2018).

[23] R. H. Swendsen and J.-Sh. Wang, Nonuniversal Critical Dynamics in Monte Carlo Simulations, Phys. Rev. Lett. **58**, 86 (1987).

[24] U. Wolff, Collective Monte Carlo Updating for Spin Systems, Phys. Rev. Lett. **62**, 361 (1989).

[25] A. Pelissetto and E. Vicari, Critical Phenomena and Renormalization-Group Theory, Phys. Rep. **368**, 549 (2002).

[26] K. G. Wilson and J. Kogut, The renormalization group and the ϵ-expansion, Phys. Rep. C **12**, 75 (1974).

[27] M. E. Fisher, The renormalization group in the theory of critical behavior, Rev. Mod. Phys. **46**, 597 (1974).

[28] M. E. Fisher, Renormalization group theory: Its basis and formulation in statistical physics, Rev. Mod. Phys. **70**, 653 (1998).

[29] M. Hasenbusch, A finite size scaling study of lattice models in the three-dimensional Ising universality class, Phys. Rev. B **82**, 174433 (2010).

[30] Y. Deng and H. W. J. Blöte, Constrained tricritical Blume-Capel model in three dimensions, Phys. Rev. E **70**, 046111 (2004).

[31] H. W. J. Blöte, L. N. Shchur, and A. L. Talapov, The Cluster Processor: New Results, Int. J. Mod. Phys. C **10**, 1137 (1999).

[32] Y. Deng and H. W. J. Blöte, Simultaneous analysis of several models in the three-dimensional Ising universality class, Phys. Rev. E **68**, 036125 (2003).

[33] S.-K. Ma, Renormalization Group by Monte Carlo Methods, Phys. Rev. Lett. **37**, 461 (1976).

[34] R. H. Swendsen, Monte Carlo Renormalization Group, Phys. Rev. Lett. **42**, 859 (1979).

[35] G. S. Pawley, R. H. Swendsen, D. J. Wallace, and K. G. Wilson, Monte Carlo renormalization-group calculations of critical behavior in the simple-cubic Ising model, Phys. Rev. B **29**, 4030 (1984).

[36] C. F. Baillie, R. Gupta, K. A. Hawick, and G. S. Pawley, Monte Carlo renormalization-group study of the three-dimensional Ising model, Phys. Rev. B **45**, 10438 (1992).

[37] H. W. J. Blöte, J. R. Heringa, A. Hoogland, E. W. Meyer, and T. S. Smit, Monte Carlo Renormalization of the 3D Ising Model: Analyticity and Convergence, Phys. Rev. Lett. **76**, 2613 (1996).

[38] M. Patra and M. Karttunen, Stencils with isotropic discretization error for differential operators, Numer. Methods Partial Differential Equations **22**, 936 (2006).

[39] M. Hasenbusch, Variance-reduced estimator of the connected two-point function in the presence of a broken $\mathbb{Z}_2$-symmetry, Phys. Rev. E **93**, 032140 (2016).

[40] M. Hasenbusch, Thermodynamic Casimir effect: Universality and corrections to scaling, Phys. Rev. B **85**, 174421 (2012).

[41] A. M. Ferrenberg, J. Xu, and D. P. Landau, Pushing the limits of Monte Carlo simulations for the three-dimensional Ising model, Phys. Rev. E **97**, 043301 (2018).

[42] M. Saito and M. Matsumoto, SIMD-oriented Fast mersenne twister: A 128-bit pseudorandom number generator, in *Monte Carlo and Quasi-Monte Carlo Methods 2006*, edited by A. Keller, S. Heinrich, and H. Niederreiter (Springer, Berlin, 2008); M. Saito, Masters thesis, Graduate School of Science, Hiroshima University, 2007. The source code of the program is provided at http://www.math.sci.hiroshima-u.ac.jp/~m-mat/MT/SFMT/index.html.

[43] P. Virtanen, R. Gommers, T. E. Oliphant, M. Haberland, T. Reddy, D. Cournapeau, E. Burovski, P. Peterson, W. Weckesser, J. Bright *et al.*, SciPy 1.0–fundamental algorithms for scientific computing in Python, Nat. Methods **17**, 261 (2020).

[44] J. D. Hunter, Matplotlib: A 2D Graphics Environment, Comput. Sci. Eng. **9**, 90 (2007).

[45] J. Salas and A. D. Sokal, Universal amplitude ratios in the critical two-dimensional Ising model on a torus, J. Stat. Phys. **98**, 551 (2000).

[46] M. Lüscher, A portable high-quality random number generator for lattice field theory simulations, Comput. Phys. Commun. **79**, 100 (1994).

[47] F. Kos, D. Poland, D. Simmons-Duffin, and A. Vichi, Precision islands in the Ising and $O(N)$ models, J. High Energy Phys. 08 (2016) 036.

[48] M. V. Kompaniets and E. Panzer, Minimally subtracted six-loop renormalization of ϕ^4-symmetric theory and critical exponents, Phys. Rev. D **96**, 036016 (2017).

[49] G. De Polsi, I. Balog, M. Tissier, and N. Wschebor, Precision calculation of critical exponents in the $O(N)$ universality classes with the nonperturbative renormalization group, Phys. Rev. E **101**, 042113 (2020).

[50] G. Gori and A. Trombettoni, Geometry of bounded critical phenomena, J. Stat. Mech.: Theory Exp. (2020) 063210.

[51] S. Vigna, It is high time we let go of the Mersenne Twister, arXiv:1910.06437.

[52] ranlux-3.4 https://luscher.web.cern.ch/luscher/ranlux/.

[53] G. G. Rose, KISS: A bit too simple, Cryptography Commun. **10**, 123 (2017).

[54] https://en.wikipedia.org/wiki/KISS_(algorithm), https://de.wikipedia.org/wiki/KISS_(Zufallszahlengenerator).

[55] https://prng.di.unimi.it/.

[56] D. Blackman and S. Vigna, Scrambled linear pseudorandom number generators, arXiv:1805.01407.

[57] https://www.pcg-random.org/posts/does-it-beat-the-minimal-standard.html.

[58] P. L'Ecuyer and R. Simard, TestU01: A software library in ANSI C for empirical testing of random number generators, ACM Trans. Math. Software **33**, 22 (2007).